IEEE Access
Multidisciplinary ⋮ Rapid Review ⋮ Open Access Journal

Received 24 August 2023, accepted 12 September 2023, date of publication 18 September 2023,
date of current version 25 September 2023.

Digital Object Identifier 10.1109/ACCESS.2023.3316263

APPLIED RESEARCH

Nonlinear Model Predictive Control Based Adaptive Equivalent Consumption Minimization Strategy for Fuel Cell Electric Bus Considering Average Travel Speed

JOOIN LEE[1] AND HYEONGCHEOL LEE[2], (Member, IEEE)
[1]Department of Electrical Engineering, Hanyang University, Seoul 04763, South Korea
[2]Department of Electrical and Biomedical Engineering, Hanyang University, Seoul 04763, South Korea

Corresponding author: Hyeongcheol Lee (hclee@hanyang.ac.kr)

This work was supported by the Korea Institute of Energy Technology Evaluation and Planning (KETEP) funded by the Korean Government [Ministry of Trade, Industry and Energy (MOTIE)] through the Development and Demonstration of Optimized Fuel-Cell Hybrid System Technology for Hydrogen Bus under Grant 20223030030010.

ABSTRACT This paper presents nonlinear model predictive control based adaptive equivalent consumption minimization strategy for fuel cell hybrid electric bus. The proposed strategy considers the average travel speed profile of road segments in route of fuel cell hybrid electric bus. The proposed nonlinear model predictive control based adaptive equivalent consumption minimization strategy determines the optimal control input by considering the battery current-rate and the fuel cell balance-of-plant. The nonlinear model predictive control based adaptive equivalent consumption minimization strategy consists of three main stages: the data pre-processing stage, the nonlinear model predictive control stage, and the adaptive equivalent consumption minimization strategy stage. In the data preprocessing stage, reference power trajectory is generated while considering the response time of the fuel cell hybrid electric bus. In the nonlinear model predictive control stage, the reference state of charge trajectory is generated by considering the battery current-rate and the fuel cell balance-of-plant. In the adaptive equivalent consumption minimization strategy stage, the optimal control input is determined to minimize instantaneous equivalent fuel consumption by considering the reference state of charge trajectory. The proposed energy management system is compared with dynamic programming using actual bus route based real-driving scenarios. The comparison results demonstrate that the proposed energy management system can generate control inputs that are similar to the global optimal solution calculated by dynamic programming with a reasonable computation time.

INDEX TERMS Nonlinear programming (NLP), model predictive control (MPC), equivalent consumption minimization strategy (ECMS), fuel cell hybrid electric vehicle (FCHEV), fuel cell hybrid electric bus (FCHEB), average travel speed.

I. INTRODUCTION

A. BACKGROUND

The overuse of fossil fuels is contributing to excessive greenhouse gas emissions, accelerating air pollution and global warming. In response to these environmental concerns, environmental regulations are getting tighter in many countries. Representatively, the National Highway Traffic Safety Administration (NHTSA) in United States has established a Corporate Average Fuel Economy (CAFE) standard that mandates to achieve an average fuel economy of 23.2 mpg by 2025 [1], [2]. In response to these environmental regulations, automotive industry has been investing significant resources in eco-friendly vehicles and development of electric vehicles has been one of top priorities.

The associate editor coordinating the review of this manuscript and approving it for publication was Wencong Su.

Due to the low energy density of batteries compared to internal combustion engines, the short driving range is the primary disadvantage of battery-based electric vehicles (BEV). Therefore, fuel cells have risen as a new power source for electric vehicles because they are emission-free mobility with high energy density. However, the fuel cells have a relatively slow response time when changes in driving load, such as sudden acceleration or deceleration are made. Also, they require a considerable amount of time to initiate and generate sufficient power at cold starts. There is a growing interest in the fuel cell hybrid electric vehicles (FCHEV), which integrate both fuel cell and battery, to overcome the limitations of both power sources.

The FCHEV combines merits of above two vehicles: the quick response time of battery, the long driving range, and rapid charging speed of fuel cell. This indicates that the FCHEV is suitable for city buses, which require long driving ranges and responsiveness to frequent change in driving load, such as stopping, accelerating, and decelerating. Therefore, fuel cell hybrid electric city buses (FCHEB) are spotlighted for their potential to establish an eco-friendly and sustainable public transportation system in urban areas. The FCHEB can operate the fuel cell and battery in high-efficiency areas and utilize regenerative braking, which recovers kinetic energy [3]. For instance, FCHEB models like Hyundai's Elec-city and Universe have been introduced to the market [4].

In order to maximize performance of FCHEB, the energy management strategy (EMS) is crucial as it determines the power distribution ratio between the fuel cell and battery to minimize energy losses.

B. LITERATURE REVIEW

EMS for FCHEV can be categorized into rule-based and optimization-based approaches. The rule-based EMS is a method that controls the vehicle according to pre-designed conditions and rules, which are designed based on the experience of engineers. The rule-based EMS has an intuitive and simple structure with low computational load, making it suitable for real-time system design and operation. In other words, it ensures high stability and robustness by relying on fixed decision rules. Representative rule-based EMS include state machine-based [5] and fuzzy logic-based [6], [7], [8]. However, the rule-based EMS may not effectively respond to dynamic changes or complex driving conditions. As a result, it can lead to inefficient utilization of the fuel cell and battery, as the rule-based EMS does not generate optimal power distribution inputs, affecting overall vehicle performance and fuel economy.

The optimization-based EMS is a methodology that utilizes optimization theory or algorithms to compute optimal control inputs. The optimization-based EMS has an unintuitive and complex structure with high computational load, which makes it difficult to design real-time system. Despite these problems, the optimization-based EMS has the capability to generate optimal control inputs that minimize fuel consumption while maximizing driving range. Its eco-friendly attributes, which contributes to the reduction of air pollution and greenhouse gas emissions, has attracted significant interest. Moreover, advance in intelligent intersection systems (ITS) and autonomous driving technologies have accelerated abundance of traffic and driving information, stimulating further research in this field. Depending on the applied optimization theory, the optimization-based EMS can be categorized into offline and online optimization algorithms.

The first is offline optimization algorithm. An offline optimization algorithm is an approach that finds the global optimal solution based on known driving conditions, such as vehicle speed and road gradient. The most popular algorithm is dynamic programming (DP). DP [9], [10], [11] involves decomposing a given complex problem into smaller subproblems and computing the optimal solutions for these subproblems to calculate the global optimal solution. However, computational complexity is very high because it calculates the solutions for all the subproblems sequentially. Additionally, DP has limitations in its ability to adapt to real-time driving condition change because it precomputes the optimal solution based on given driving conditions. Therefore, it is primarily used as a benchmark for evaluating the performance of other EMSs.

The second is online optimization algorithm. An online optimization algorithm is an approach that finds the local optimal solution when driving condition is changing dynamically. It must ensure low computational complexity, stability, and robustness because it calculates optimal solution at each control period using limited computational resources available in the hybrid control unit (HCU). Representative online optimization algorithms include pontryagin's minimum principle (PMP), equivalent consumption minimization strategy (ECMS), and model predictive control (MPC), etc. PMP [12], [13], [14], [15] involves deriving the Hamiltonian function from the constraints and the cost function. It establishes necessary conditions for optimality based on Hamiltonian function. By satisfying these necessary conditions, PMP calculates the optimal control input. ECMS [16], [17], [18] calculates the equivalent energy consumption and determines the optimal control inputs that minimize the cost function. However, accurately determining the equivalent factor, the cost difference between the fuel cell and battery, is challenging because it varies dynamically according to change in driving conditions. Therefore, the adaptive-ECMS (A-ECMS) [19], [20], [21], [22] algorithm has been proposed, as it can adjust the equivalent factor according to various driving conditions. MPC [23], [24], [25], [26], [27] utilizes a mathematical model of the target system to predict its future state over a specific time horizon. It employs numerical methods to calculate optimal inputs that minimize a cost function, considering the predicted state trajectory.

Recently, various EMS have been proposed by combining the afore mentioned methods to leverage advantages of each method. Li et al. [28] proposed a multi-objective

MPC-based EMS that aims to enhance the fuel cell durability and lifetime while minimizing fuel consumption. The cost function of the proposed MPC consists of three terms: instantaneous fuel consumption, fuel cell stress, and battery stress. In multi-objective MPC, assigning suitable weights to these terms is important to accurately respond to the driving conditions. The proposed multi-object MPC-based EMS utilized fuzzy logic to determine the appropriate weights for the driving conditions. Lin et al. [29] proposed an A-ECMS based EMS for a plug-in fuel cell electric vehicle (FCEV). The proposed A-ECMS uses multivariate nonlinear regression (MNLR) and sequential quadratic programming (SQP) to update the equivalent factor. The proposed ECMS is validated by comparison with the existing ECMS methods in simulation environment, which is a combined driving cycle including the New York City cycle (NYCC), urban driving dynamometer schedule (UDDS) and highway fuel economy test cycle (HWFET). Yan et al. [30] proposed a hierarchical predictive EMS (HPEMS) for FCHEV. The HPEMS consists of two levels: the upper-level determines the optimal launch time based on traffic and vehicle states using deep reinforcement learning (DRL), while the lower-level employs MPC to determine the power distribution ratio between the fuel cell and battery. The proposed HPEMS aims to reduce energy consumption and travel time by considering the energy loss caused by frequent starting and stopping at intersections. Salem et al. [31] proposed a multi-objective online optimization-based EMS. The cost function of the proposed EMS consists of four terms: instantaneous fuel consumption, fuel cell stress, battery stress, and the penalty for deviations from the desired State of Charge (SOC) of the battery. The cost function in the multi-objective online optimization-based EMS is formulated as a quadratic form with linear constraints. The Hildreth algorithm, which is an iterative optimization algorithm used to solve quadratic programming (QP), is employed to calculate the optimal control input. The proposed EMS is validated by comparing it with the results obtained using DP for the New European Driving Cycle (NEDC) and US06 scenarios.

The above research has made significant contributions to the advancement of EMS for FCHEV. Specifically, the EMS based on A-ECMS and MPC was proven to be well-suited as an online optimization algorithm, since various driving conditions are taken into consideration when calculating optimal control inputs. However, there are three additional aspects that need to consider in an EMS when it is applied to FCHEB.

- First, the FCHEB currently operating in urban areas where autonomous driving capabilities are not equipped. Consequently, the EMS cannot use the precise speed profile to calculate the optimal control input. The lack of information on speed profile is detrimental to the performance of the EMS. Hence, it is crucial to include even limited information, such as the average speed obtained from the navigation system, to minimize fuel consumption throughout the route.
- Second, city buses experience frequent start-and-stop cycles due to traffic congestion, intersections, and bus stops. These repetitive operations have a negative impact on the durability of the fuel cell and battery. The balance-of-plant (BOP), which includes components like pumps and humidifiers, plays a crucial role in maintaining the durability of the fuel cell. Additionally, the current-rate (C-rate), which regulates the charging and discharging rate of the battery, significantly influences its durability. Therefore, when calculating the optimal control input, the EMS of the FCHEB must consider both the C-rate and BOP.
- Third, the performance of the EMS for FCHEB should be validated by comparing it to a global optimal solution using real driving scenarios rather than using standard driving cycles. City buses often follow repetitive routs, making it effective and important to analyze the performance of EMS under real driving scenarios.

C. MAIN CONTRIBUTION

The main objective of this paper is to develop the EMS for FCHEB that considers the average travel speed of the road. The main contributions are listed as follows:

- First, a hierarchical nonlinear control framework is proposed in this study, where nonlinear MPC (NMPC) is employed at the high-level and A-ECMS is used at the low-level. Unlike previous research, the NMPC generates a reference SOC trajectory that considers the average travel speed of the road.
- Second, the NMPC with the interior point method (IPM) is utilized to generate the reference SOC trajectory, considering the average travel speed of the roads along the route of the target city bus. The prediction model and constraints are designed to incorporate the characteristics of the BOP and C-rate, while the cost function is formulated to minimize fuel consumption of the fuel cell. And the A-ECMS calculates the optimal power distribution ratio between the fuel cell and battery by considering the accelerator/brake pedal input. The A-ECMS adjusts the equivalent factor based on the reference SOC trajectory calculated by the NMPC.
- Third, the proposed NMPC-based A-ECMS is validated, by comparing it with the global optimal results of DP. It is validated on the real driving scenarios, which were measured by RT3100 device, with diverse traffic environments. These real driving scenarios consist of four driving situations, which include the road environment of two city bus routes and the traffic environment at two different time periods.

The remainder of this paper is organized as follows. Section II. describes the vehicle model of target FCHEB. Section III. introduces the NMPC-based A-ECMS, which consists of the NMPC at the high-level and A-ECMS at the

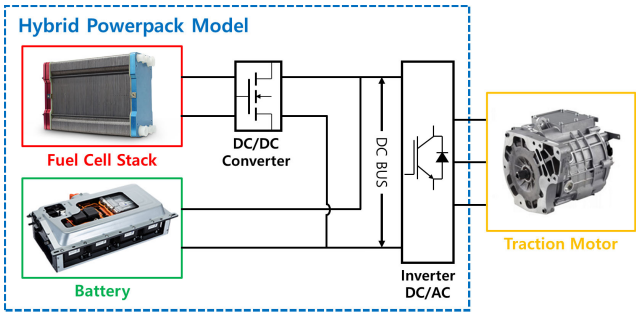

FIGURE 1. Powertrain topology of FCHEB, which operate in three modes, namely fuel cell-only mode, battery-only mode, and hybrid mode. This is designed to allow the fuel cell stack to generate additional power to meet power requirements, while saving excess power in the battery. The FCHEB can charge the battery in either hybrid or fuel cell-only mode using power from the fuel cell stack.

TABLE 1. Component specifications of the FCHEB.

Component	Parameter	Value
Traction Motor	Maximum Power	180 kW
Fuel Cell Stack	Maximum Power	180 kW
Battery	Capacity	120 Ah
	Voltage	654 V
Wheel	Wheel Radius	0.47 m
Chassis	Mass	12655 kg

low-level. Section IV. analyzes the simulation results and validates the performance of the proposed EMS. Finally, Section V. summarizes the conclusions and discusses future work.

II. VEHICLE MODEL

This section describes the system model for the vehicle targeted in this paper. The target vehicle is a FCHEB, consisting of a fuel cell stack, battery, traction motor, as shown in Figure 1. The detailed specifications of the target FCHEB are shown in Table 1. The system model described in this section is a type of control-oriented model that is used for NMPC and A-ECMS.

A. VEHICLE DYNAMICS

The longitudinal vehicle dynamics model is used to calculate the demand power, which is required to drive the vehicle. First, the wheel torque is calculated using the driving speed and road gradient, as shown in (1). The wheel torque represents the torque required when tracking the target speed, considering acceleration force, air drag force, gradient force, and rolling resistance force. The wheel speed is calculated by the longitudinal vehicle chassis speed, as shown in (2). T_w is the wheel torque, γ_w is the wheel radius, m is the vehicle mass, v is the vehicle speed, ρ is the air density, A_f is the frontal area, C_a is the drag coefficient, g is the gravitational acceleration, θ is the road gradient, C_r is the rolling coefficient, and ω_w is the wheel speed.

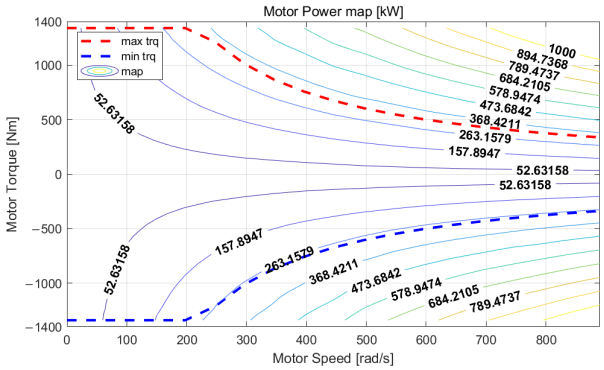

FIGURE 2. Motor power map for charging and discharging. The red line indicates the maximum torque of the motor, while the blue line represents the minimum torque of the motor.

$$T_w = \gamma_w(m\frac{dv}{dt} + \frac{1}{2}\rho A_f C_a v^2 + mg\sin\theta + mgC_r) \quad (1)$$

$$\omega_w = v\frac{1}{\gamma_w} \quad (2)$$

Second, the motor torque is calculated using the gear ratio and efficiency of the final drive gear, as shown in (3). In the FCHEB, the motor is connected to the wheels through the final drive gear. The motor speed is calculated by the wheel speed, as shown in (4). The motor torque and motor speed represent the required torque and speed for the motor to propel the vehicle using energy from the fuel cell and battery. T_{mot} is the motor torque, f_{trq} is the function for the motor torque, ω_{mot} is the motor torque, f_{spd} is the function for the motor speed, η_{fd} is the final drive gear efficiency, and γ_{fd} is the final drive gear ratio.

$$T_{\text{mot}} = f_{\text{trq}}(v,\theta) = \begin{cases} T_w\eta_{\text{fd}}\dfrac{1}{\gamma_{\text{fd}}}(T_w < 0) \\ T_w\dfrac{1}{\eta_{\text{fd}}}\dfrac{1}{\gamma_{\text{fd}}}(T_w >= 0) \end{cases} \quad (3)$$

$$\omega_{\text{mot}} = f_{\text{spd}}(v) = \omega_w\gamma_{\text{fd}} \quad (4)$$

Third, the motor power is obtained from the map, as shown in Figure 2. The motor power map represents the relationship between torque and speed, considering the efficiency of motor, as shown in (5). The motor power is the demand power required by the vehicle to track the reference speed. f_{pwr} is the function for the motor torque.

$$P_{\text{mot}} = f_{\text{pwr}}(T_{\text{mot}}, \omega_{\text{mot}}) \quad (5)$$

B. FUEL CELL STACK

The fuel cell generates electrical power through a chemical reaction involving hydrogen and oxygen. However, due to the complexity and high uncertainty of the chemical reaction, they are not directly used in the EMS. Instead, the proposed EMS relies on a control-oriented model that represents the relationship between fuel cell power and fuel consumption rate, as shown in Figure 3.

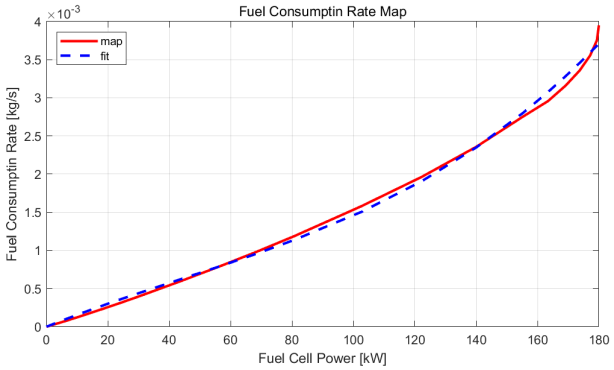

FIGURE 3. Fuel consumption rate map. The fuel consumption rate is closely related to the power of the fuel cell. As the fuel cell outputs more power, a higher fuel consumption rate is required. However, this relationship is not linear, because it reflects the efficiency of the fuel cell.

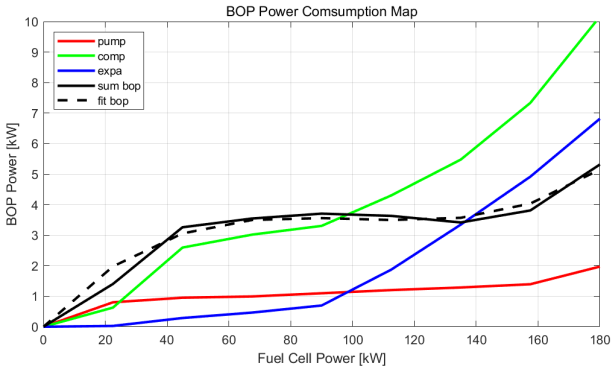

FIGURE 4. BOP power map. The power consumption of the pump, compressor, and expander is represented by the red, green, and blue lines, respectively. The solid black line represents the BOP power map, which is the sum of the power consumption of the pump, compressor, and expander. The dashed black line represents the polynomial function approximating the BOP power map.

The proposed EMS determines the optimal control input to minimize fuel consumption, which is calculated through the integration of the fuel consumption rate. To formulate the fuel consumption rate map as an optimal control problem (OCP) for the NMPC, it is necessary to represent the map as a polynomial function, as illustrated in (6). The comparison between the polynomial function (represented by the dashed blue line) and the original map (represented by the solid red line) is illustrated in Figure 3. $\dot{m}_{\mathrm{fc}}$ is the fuel consumption rate, P_{fc} is the fuel cell power, and c_3 / c_2 / c_1 / c_0 are coefficients of the polynomial.

$$\dot{m}_{\mathrm{fc}}(P_{\mathrm{fc}}) = c_3 P_{\mathrm{fc}}^3 + c_2 P_{\mathrm{fc}}^2 + c_1 P_{\mathrm{fc}} + c_0 \tag{6}$$

The BOPs are the auxiliary devices that are related to the supporting systems, which is required for the reliable operation of the fuel cell stack. These components are responsible for functions such as fuel delivery, air delivery, cooling management, and control of valves and switches. The operation of the BOP, which is crucial for ensuring the durability and reliability of the fuel cell stack, requires the consumption of electrical power. Therefore, it is necessary to consider the electrical power consumed by the BOP to optimize the energy consumption of the FCHEB.

In this paper, we focus on three key components of the BOP: pump, compressor, and expander. The pump, which is part of the fuel supply system, maintains the pressure of the fuel and delivers it to the stack. The compressor intakes, compresses, and delivers air to the stack as part of the air supply system. The expander is responsible for efficient heat management within the fuel cell stack. It utilizes the waste heat energy from the exhaust gases of the stack to recover electrical energy. The power consumed by the BOP is dependent on the fuel cell power, as shown in Figure 4. The BOP is used to calculate the demand power, which must be generated by the fuel cell stack and battery, as shown in (7)–(8). To incorporate the BOP power map into the OCP of the NMPC, it is essential to represent the map as a polynomial function, as shown in (9). Figure 4 illustrates the comparison between the polynomial function (represented by the dashed black line) and the original map (represented by the solid black line). P_{bop} is the BOP power, P_{pump} is the pump power, P_{comp} is the compressor power, P_{expa} is the expander power, P_{dmd} is the demand power, η_{dc} is the efficiency of dc/dc converter, P_{bat} is the battery power, and a_3 / a_2 / a_1 are coefficients of the polynomial.

$$P_{\mathrm{bop}} = P_{\mathrm{pump}} + P_{\mathrm{comp}} - P_{\mathrm{expa}} \tag{7}$$

$$P_{\mathrm{dmd}} = P_{\mathrm{mot}} + P_{\mathrm{bop}} = \eta_{\mathrm{fc}} P_{\mathrm{fc}} + P_{\mathrm{bat}} \tag{8}$$

$$P_{\mathrm{bop}} = a_3 P_{\mathrm{fc}}^3 + a_2 P_{\mathrm{fc}}^2 + a_1 P_{\mathrm{fc}} \tag{9}$$

C. BATTERY

The internal resistance model, which is a control-oriented battery model, is utilized to calculate the SOC. This model calculates the battery SOC by defining the equivalent circuit by considering internal resistance, open-circuit voltage, and motor power, as shown in (10). I_{bat} is the battery current, V_{oc} is the open-circuit voltage, and R_{int} is the internal resistance.

$$I_{\mathrm{bat}} = \frac{V_{\mathrm{oc}} - \sqrt{V_{\mathrm{oc}}^2 - 4R_{\mathrm{int}}P_{\mathrm{bat}}}}{2R_{\mathrm{int}}} \tag{10}$$

The open-circuit voltage and internal resistance of a battery are functions of the SOC. To formulate the SOC as an OCP for the NMPC, it is necessary to translate the open-circuit voltage map and internal resistance map into equation, as illustrated in (11)–(12). q_3 / q_2 / q_1 / q_0 are coefficients of the open-circuit voltage, and r_3 / r_2 / r_1 / r_0 are coefficients of the internal resistance.

$$V_{\mathrm{oc}} = q_3 \mathrm{SOC}^3 + q_2 \mathrm{SOC}^2 + q_1 \mathrm{SOC} + q_0 \tag{11}$$

$$R_{\mathrm{int}} = r_0 \exp(-r_1 \mathrm{SOC}) + r_2 \exp(-r_3 \mathrm{SOC}) \tag{12}$$

The battery SOC is calculated by integrating the current used by the battery, as shown in (13). Q_{bat} is the battery capacity.

$$\dot{\mathrm{SOC}} = -\frac{I_{\mathrm{bat}}}{Q_{\mathrm{bat}}} = -\frac{V_{\mathrm{oc}} - \sqrt{V_{\mathrm{oc}}^2 - 4R_{\mathrm{int}}P_{\mathrm{bat}}}}{2R_{\mathrm{int}}Q_{\mathrm{bat}}} \tag{13}$$

The C-rate of a battery represents its relative charging or discharging rate to its capacity, as shown in (14). It is

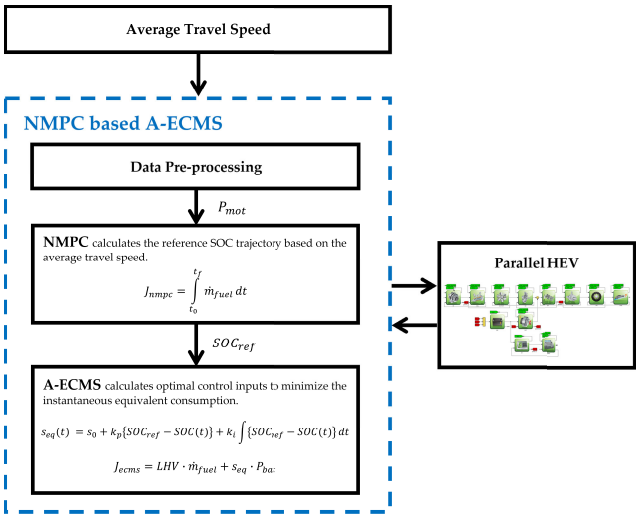

FIGURE 5. The concept diagram of the NMPC based ECMS for FCHEB considering average travel speed.

calculated as the ratio of the current to the battery capacity, which indicates number of times that the battery capacity can be charged or discharged within a specific time. The C-rate is a critical factor when determining the maximum charge or discharge current that the battery can safely handle. Therefore, it is essential to consider the C-rate when calculating the optimal input to ensure the durability of the battery. C_{rate} is the battery C-rate, and $I_{\max}$ is the maximum battery current.

$$C_{\text{rate}} = \frac{I_{\max}}{Q_{\text{bat}}} \tag{14}$$

III. NONLINEAR MODEL PREDICTIVE CONTROL BASED ADAPTIVE EQUIVALENT CONSUMPTION MINIMIZATION STRATEGY

This section presents a description of the hierarchical nonlinear control framework for the proposed NMPC-based A-ECMS. The structure of the NMPC-based A-ECMS is illustrated in Figure 5. The NMPC-based A-ECMS's optimal control input calculating process can be divided in to 3 stages: the data pre-processing stage, the NMPC stage, and A-ECMS stage.

The proposed NMPC-based A-ECMS utilizes the average travel speed of the road segment, which represents the speed of the traffic flow rather than the speed of individual vehicles. The average travel speed indicates the typical range of speed at which the vehicle generally travels. The grade of the road influences the driving resistance of the vehicle. Both the average travel speed and the grade of the road are major factors that impact fuel economy significantly [32], [33]. This information represents the specific driving pattern, which can influence the fuel economy of a vehicle. It is important that equivalent factor of A-ECMS reflects these driving patterns because it represents the difference in energy value between the fuel cell and battery under specific driving conditions.

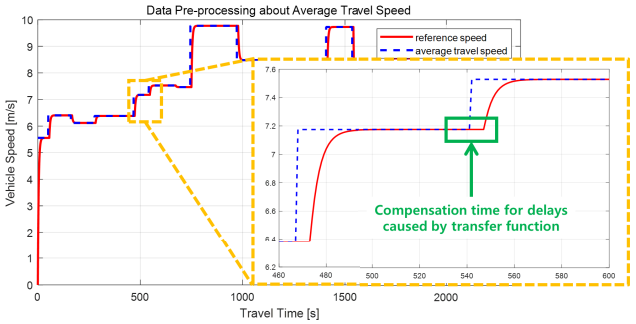

FIGURE 6. The result of calculating the reference speed profile using the average travel speed profile based on the travel time. The reference speed profile considers the delay time of the FCHEB system. It also compensates for the difference between the travel distance and the length of the road segment due to the delay.

A. DATA PRE-PROCESSING

The data pre-processing stage generates the reference power trajectory by considering the average travel speed profile of each road segment along the path of the FCHEB. The reference power trajectory is used to determine the appropriate equivalent factor for the road traffic environment. The reference power trajectory is calculated in three steps.

The first step is to create a travel time-based average travel speed profile. The average travel speed profile is distance-based profile because it represents the average speed values assigned to the road segments included in the FCHEB route. However, the average speed profile must be a travel time-based profile when it is used in the EMS. The estimated travel time is calculated by the length and average speed of each road segments, as shown in (15). As a result, the travel distance-based average speed profile is transformed into the travel time-based average speed profile by taking into account the length and average speed of each road segment. $t_{\text{trav.i}}$ is the travel time of the i^{th} road segment, $l_{\text{road.i}}$ is the length of the i^{th} road segment, and $v_{\text{avg.i}}$ is the average speed of the i^{th} road segment.

$$t_{\text{trav.i}} = \frac{l_{\text{road.i}}}{v_{\text{avg.i}}} \tag{15}$$

The second step is generating the reference speed profile that reflects the characteristics of the FCHEB. The average travel speed profile is not differentiable because of its discrete characteristics. It is discontinuous because single value representing the average speed is assigned to each road segment. However, the differentiation of the average travel speed profile is necessary to calculate the acceleration force to generate the reference power trajectory. Therefore, the average travel speed profile is smoothed using a transfer function model that represents the delay time of the FCHEB system, including factors such as driver response and actuator dynamics. The FCHEB is modeled as a first-order system, which represents the delay time of the vehicle, to simplify the calculation process [34], [35]. The PD controller is applied to the first-order system to track the average travel speed profile. The simplified FCHEB model with PD controller, which is used in data pre-processing stage, is expressed as (16). The

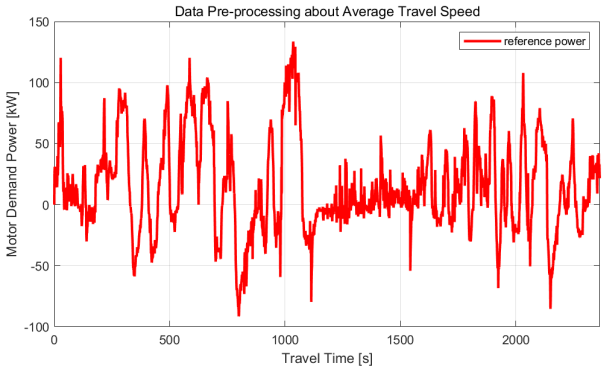

FIGURE 7. The result of calculating the reference power profile based on the travel time using the reference speed profile.

average travel speed profile based on the travel time and the smoothed reference speed profile are shown in Figure 6. G(s) is the transfer function that takes the average travel speed and generates a vehicle speed as output, k_p is the P-gain of the PD controller, k_d is the D-gain of the PD controller, and τ_v is the delay time of the FCHEB.

$$G(s) = \frac{k_d s^2 + k_p s}{s^2(\tau_v s + 1) + (k_d s^2 + k_p s)} \tag{16}$$

The third step is calculating the reference power trajectory based on the reference speed profile and the road grade. This trajectory represents the demand motor power calculated based on a reference speed and grade profile, as shown in (17). $P_{\text{ref.mot}}$ is the reference power trajectory, v_{ref} is the reference speed profile, and θ_{ref} is the grade profile. The grade profile is determined based on the map information and the travel distance, which is calculated using the reference speed profile.

$$P_{\text{ref.mot}} = f_{\text{pwr}}\left\{f_{\text{trq}}(v_{\text{ref}}, \theta_{\text{ref}}), f_{\text{spd}}(v_{\text{ref}})\right\} \tag{17}$$

B. NONLINEAR MODEL PREDICTIVE CONTROL

The NMPC stage calculate the reference SOC trajectory considering the reference power trajectory, BOP, and C-rate. The objective of NMPC is to compute the reference SOC trajectory that minimizes fuel consumption. This reference SOC trajectory is used as an input by the A-ECMS to determine the optimal control input. It is important that NMPC computes accurate reference SOC trajectory over longer time horizon within a reasonable computation time.

For NMPC to compute the reference SOC trajectory, the OCP consists of a cost function and constraints, should be formulated. The cost function is a mathematical representation of the optimization objective. The proposed NMPC aims to minimize the fuel consumption, as shown in (18). J_{nmpc} is the cost function for the NMPC.

$$J_{\text{nmpc}} = \int_{t_0}^{t_f} \dot{m}_f(P_{\text{fc}}) \tag{18}$$

The constraints are used to ensure that the NMPC considers the physical characteristics of the FCHEB, which are represented by the state equation. Therefore, the proposed NMPC includes equality constraints on the state equation for the battery SOC, as shown in (19). The state equation incorporates the battery power, which is calculated based on the reference power trajectory obtained from the data pre-processing stage. The reference power trajectory serves as a constraint that the battery power and fuel cell power must satisfy. This trajectory represents the demand power required by the motor. When utilizing the fuel cell power, it is essential to consider the power consumed by the BOP and the DC/DC converter to maintain durability. Therefore, the formula used for the battery power determination needs to include terms accounting for the BOP and the DC/DC converter, as shown in (20). The state equation is discretized using the Euler method, as shown in (21). The initial values play a crucial role in model prediction using the state equation. Therefore, the initial value for the battery SOC is set as a constraint, as shown in (22). x_{nmpc} is the state of the prediction model in NMPC, f_{nmpc} is the state equation for the NMPC, k is the step, t_{step} is the step time or step size for the NMPC, t_0 is the initial time, and SOC_0 is the initial value of SOC.

$$\dot{x}_{\text{nmpc}} = f_{\text{nmpc}} = \frac{V_{\text{oc}} - \sqrt{V_{\text{oc}}^2 - 4R_{\text{int}}P_{\text{bat}}}}{2R_{\text{int}}} \tag{19}$$

$$P_{\text{bat}} = P_{\text{ref.mot}} + a_3 P_{\text{fc}}^3 + a_2 P_{\text{fc}}^2 + (a_1 - \eta_{\text{dc}})P_{\text{fc}} \tag{20}$$

$$x_{\text{nmpc}}\left[k+1\right] = x_{\text{nmpc}}\left[k\right] + t_{\text{step}} f_{\text{nmpc}} \tag{21}$$

$$x_{\text{nmpc}}\left[t_0\right] = \text{SOC}_0 \tag{22}$$

The constraints ensure that the NMPC can operate within certain limits of inputs and states variables. The proposed NMPC includes inequality constraints on the state variables, state derivatives, input variables, and input derivatives. If the SOC remains too low or too high, it can lead to capacity degradation and reduced battery lifespan. Therefore, the NMPC includes inequality constraints to maintain the SOC within a certain range during the control horizon, as shown in (23). Typically, the SOC is kept between 20% and 80% throughout the control horizon. However, to ensure energy reserve and prepare for unexpected situations, in the last time of the control horizon, NMPC needs to maintain the SOC above a specific value, such as 60%, as shown in (24). SOC_{min} is the minimum boundary for the SOC, SOC_{max} is the maximum boundary for the SOC, $SOC_{fin.min}$ is the minimum boundary for the SOC at the final time, $SOC_{fin.max}$ is the maximum boundary for the SOC at the final time, and t_f is the final time.

$$\text{SOC}_{\text{min}} <= x_{\text{nmpc}}\left[k\right] <= \text{SOC}_{\text{max}} \tag{23}$$

$$\text{SOC}_{\text{fin.min}} <= x_{\text{nmpc}}\left[t_f\right] <= \text{SOC}_{\text{fin.max}} \tag{24}$$

If the battery is charged or discharged with a current exceeding its maximum limit, it can result in performance degradation and safety issues. Therefore, the NMPC includes inequality constraints on the current used for charging or

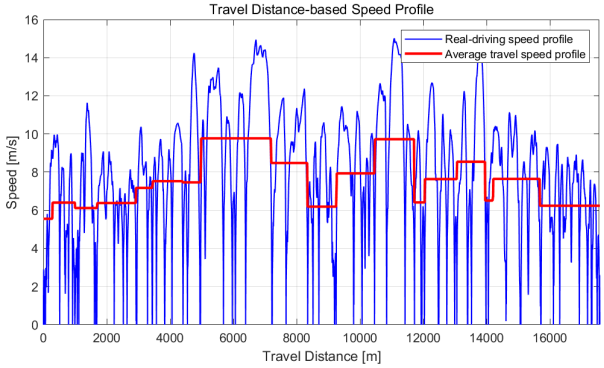

FIGURE 8. Comparison of the travel distance-based reference speed profile. The blue line indicates the real-driving speed profile used by DP to calculate the reference SOC trajectory. The red line indicates the average travel speed profile used by NMPC to calculate the reference SOC trajectory.

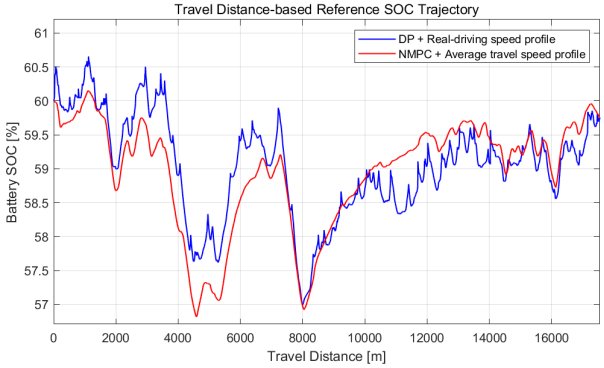

FIGURE 9. Comparison of the travel distance-based reference SOC trajectory. The blue line represents the DP result based on the real driving speed profile. The red line represents the NMPC result based on the average travel speed profile.

discharging. Since the proposed NMPC does not directly consider the battery current as a state variable, it limits the maximum current by performing differential on the SOC, as shown in (25). The maximum/minimum rate of SOC change is determined by the maximum current, which is calculated based on the C-rate. $\Delta\mathrm{SOC}_{\min}$ is the minimum rate of change of the SOC, $\Delta\mathrm{SOC}_{\max}$ is the maximum rate of change of the SOC, and Δx_{nmpc} is the rate of change of the state.

$$\Delta\mathrm{SOC}_{\min} <= x_{\mathrm{nmpc}}\left[k\right] <= \Delta\mathrm{SOC}_{\max} \tag{25}$$

The fuel cell stack of the FCHEB is limited in its maximum power value and the rate of change of power. Therefore, the proposed NMPC includes inequality constraints on the inputs to ensure that the fuel cell power remains within a specified range during the control horizon, as shown in (26). Additionally, the fuel cell stack has a relatively slower response time compared to the battery. Therefore, the proposed NMPC includes inequality constraints on fuel cell power rate change, as shown in (27). $P_{\mathrm{fc.max}}$ is the maximum power of the fuel cell, $\Delta P_{\mathrm{fc.min}}$ is the minimum rate of change of the fuel cell power, and $\Delta P_{\mathrm{fc.max}}$ is the maximum rate of change of the fuel cell power.

$$0 <= P_{\mathrm{fc}}\left[k\right] <= P_{\mathrm{fc.max}} \tag{26}$$

$$\Delta P_{\mathrm{fc.min}} <= \Delta P_{\mathrm{fc}}\left[k\right] <= \Delta P_{\mathrm{fc.max}} \tag{27}$$

The OCP for the proposed NMPC, which considers the BOP and C-rate to maintain the durability of the fuel cell and battery, is summarized by (28). The cost function aims to minimize fuel consumption, while the state equation for the battery SOC, which takes the fuel cell power as an input, is utilized in the prediction model. The OCP is transformed into a nonlinear problem (NLP), using the direct multiple shooting method. And, the NLP is solved by an NLP solver, using the interior point method (IPM) [36], [37], [38]. x^* is the optimal control state, which includes battery SOC. u^* are the optimal control inputs, which includes fuel cell power and battery power.

$$\min_{x^*u^*} J_{\mathrm{nmpc}} = \min \int_{t_{\mathrm{h.0}}}^{t_{\mathrm{h.f}}} \dot{m}_f(P_{\mathrm{fc}})$$

$$s.t. \begin{cases} x_{\mathrm{nmpc}}[k+1] - (x_{\mathrm{nmpc}}[k] + t_{\mathrm{step}} f_{\mathrm{nmpc}}) = 0 \\ x_{\mathrm{nmpc}}[t_0] - \mathrm{SOC}_0 = 0 \\ \mathrm{SOC}_{\min} <= x_{\mathrm{nmpc}}[k] <= \mathrm{SOC}_{\max} \\ \mathrm{SOC}_{\mathrm{fin.min}} <= x_{\mathrm{nmpc}}[t_f] <= \mathrm{SOC}_{\mathrm{fin.max}} \\ \Delta\mathrm{SOC}_{\min} <= \Delta x_{\mathrm{nmpc}}[t_f] <= \Delta\mathrm{SOC}_{\max} \\ 0 <= P_{\mathrm{fc}}[k] <= P_{\mathrm{fc.max}} \\ \Delta P_{\mathrm{fc.min}} <= \Delta P_{\mathrm{fc}}[k] <= \Delta P_{\mathrm{fc.max}} \end{cases} \tag{28}$$

The reference SOC trajectory which is calculated by the NMPC is a time-based profile because it is calculated by the time-based reference power profile. The travel time, represented by the x-axis of the reference SOC trajectory, is estimated based on road length and the average speed profile. However, reference SOC trajectory must be converted into a distance-based map which uses road length as a basis, when it is utilized in A-ECMS.

The reference SOC trajectory obtained by the NMPC is shown in Figure 8 and Figure 9. The DP result calculates the reference SOC trajectory based on the real driving scenario, which is acquired by the RT3100 device. The real driving speed profile is characterized by reflecting frequent starts and stops due to traffic environment and the presence of bus stations along the route. The NMPC result computes the reference SOC trajectory by considering the average travel speed, which is computed through the data pre-processing stage. The average travel speed profile represents the speed of traffic flow, which is the average speed of the vehicles on the road. Unlike the real driving speed, the average travel speed changes in a step-like manner based on the road segments, without any stopping periods. The NMPC results exhibit similarity to that of DP, depending on the road segments. This indicates that the reference SOC trajectory is close to the global optimal solution calculated by the DP.

C. ADAPTIVE EQUIVALENT CONSUMPTION MINIMIZATION STRATEGY

The A-ECMS stage determines the optimal control input considering the reference SOC trajectory. The objective of A-ECMS is to determine the optimal control input that minimize the equivalent fuel consumption. The equivalent fuel consumption is the sum of the energy consumption of the fuel cell and the battery, considering the equivalent factor. The equivalent factor, which quantifies the energy cost difference between the fuel cell and the battery, depends on the traffic conditions and vehicle states.

The A-ECMS formulates an instantaneous cost function based on equivalent fuel consumption, as shown in (29). The grid of fuel cell power is used to determine the optimal control inputs that minimize the instantaneous cost function. The grid consists of a set of fuel cell power candidates used to determine the optimal control input. It contains a total of 181 elements, considering the maximum fuel cell power of 180 kW, as shown in (30). J_{ecms} is the cost function for the A-ECMS, S_{eq} is the equivalent factor, $P_{\text{bat.grd}}$ is the battery power calculated for the grid, $P_{\text{fc.grd}}$ is the fuel cell power calculated for the grid, and u_{grd} is the input grid used in the A-ECMS.

$$J_{\text{ecms}} = S_{\text{eq}} P_{\text{bat.grd}} + P_{\text{fc.grd}} \tag{29}$$

$$u_{\text{grd}} = P_{\text{fc}} = [0, 1, \cdots, 179, 180]_{181\times 1} \tag{30}$$

The instantaneous cost function for the candidates included in the input grid is calculated based on the fuel cell power and battery power at each moment, considering the demand power. The demand power is calculated based on the driver's accelerator pedal signal (APS) and brake pedal signal (BPS), as shown in (31). The fuel cell power for the grid is calculated by considering the fuel consumption and lower heating value (LHV) with respect to the input grid, as shown in (32). The BOP power for the grid is calculated based on the input grid and the BOP power map represented by a polynomial function, as shown in (33). The battery power for the grid is calculated based on the demand power, efficiency of the DC/DC converter, fuel cell power for the grid, and BOP power for the grid, as show in (34). P_{ecms} is the instantaneous demand power considered by A-ECMS, Q_{LHV} is the lower heating value of the fuel cell, and $P_{\text{bop.grd}}$ is the BOP power calculated for the grid.

$$P_{\text{ecms}} = P_{\text{mot}} = f_{\text{pwr}}(T_{\text{mot}}(\text{APS}, \text{BPS}), \omega_{\text{mot}}) \tag{31}$$

$$P_{\text{fc.grd}} = Q_{\text{LHV}} \dot{m}_{\text{fc}}(u_{\text{grd}}) \tag{32}$$

$$P_{\text{bop.grd}} = a_3 u_{\text{grd}}^3 + a_2 u_{\text{grd}}^2 + a_1 u_{\text{grd}} \tag{33}$$

$$P_{\text{bat.grd}} = P_{\text{ecms}} + P_{\text{bop.grd}} - \eta_{\text{dc}} P_{\text{fc.grd}} \tag{34}$$

The equivalent factor is regulated based on the reference SOC trajectory generated by NMPC. The PI controller is used to adjust the equivalent factor [39]. It calculates the equivalent factor based on the gap between the reference SOC trajectory and the current SOC state of the FCHEB, as shown in (35) and (36). SOC_{err} is the SOC error, SOC_{ref} is the reference SOC trajectory, SOC_k is the current SOC state of the FCHEB, S_0 is the initial equivalent factor, K_p is the proportional gain, and K_i is the integral gain.

$$\text{SOC}_{\text{err}} = \text{SOC}_{\text{ref}} - \text{SOC}_k \tag{35}$$

$$S_{\text{eq}} = S_0 + K_p \text{SOC}_{\text{err}} + K_i \int \text{SOC}_{\text{err}} \tag{36}$$

The proposed A-ECMS aims to determine the optimal input from the input grid that minimize the instantaneous cost function, as shown in (37). This cost function is calculated based on the equivalent fuel consumption, which considers the demand power, battery power, reference SOC trajectory, fuel cell power, and BOP.

$$\min J_{\text{ecms}} = \min \left\{ S_{\text{eq}} P_{\text{bat.grd}} + P_{\text{fc.grd}} \right\} \tag{37}$$

TABLE 2. Comparison of NMPC and the two DP methods for calculating reference SOC trajectory.

Feature	DP(1)	DP(2)	NMPC
Basic Concept	Bellman's Optimality Principle		Receding Horizon Control
Optimality	Global Optimal Solution		Local Optimal Solution
Real-time Capability	Offline		Online
Input Data	Measured Travel Speed Profile	Average Travel Speed Profile	
Control Horizon	Total Travel time	500 step	
Calculation Time	Average 14896.3 s	Average 355.78 s	Average 0.263 s

IV. SIMULATION RESULT

In this section, the performance of the proposed NMPC-based A-ECMS is validated by comparing it with the results of two different DP approaches in the model-in-the-loop simulation (MILS). The NMPC-based A-ECMS generates the reference SOC trajectory and controls the FCHEB based on the average speed profile of the road segments, which is included in the FCHEB route. The comparison between the NMPC, which generates the reference SOC trajectory of NMPC-based A-ECMS, and the two DP methods is presented in Table 2.

The first DP approach, DP(1), determines the reference SOC trajectory based on the accurate speed profile, which is obtained when precise future driving information is provided. The accurate speed profile used in the DP(1) is obtained by collecting real-world driving data using an RT3100 device. Therefore, the results obtained from the first DP approach can represent a global optimal solution since the precise future driving information, such as the speed profile and grade profile, is known in advance.

The second DP approach, DP(2), determines the reference SOC trajectory based on the average speed profile of the road

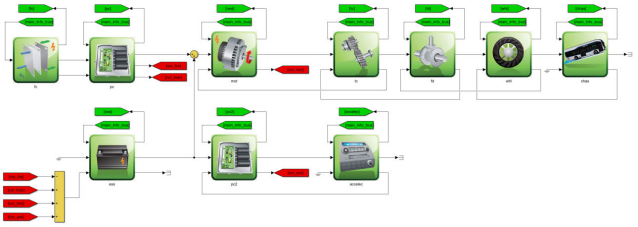

FIGURE 10. Simulation model for the FCHEB. The FCHEB simulation model is established using MATLAB, SIMULINK, and Autonomie.

segments. The second DP approach determines the reference SOC trajectory based on the average speed information over the same control horizon, which is used in the NMPC-based A-ECMS. Therefore, the result obtained by the second DP approach can be used to verify the performance of NMPC. The NMPC-based A-ECMS utilizes a control horizon of 500 steps, which corresponds with the increments in travel distance based on the average speed profile [40].

However, since DP is an offline optimization method, direct comparison is not possible. Therefore, DP-based A-ECMS was utilized, which controls the battery of the FCHEB to track the reference SOC trajectory calculated by DP, in order to evaluate and compare its performance with the NMPC-based A-ECMS.

The simulation model that incorporates the FCHEB model and NMPC-based A-ECMS is established using Autonomie, which is a forward-looking simulation tool developed by Argonne [41]. The FCHEB simulation model is illustrated in Figure 10. The desktop computer used for simulation and validation has an AMD Ryzen 5 5600X 6-core processor (3.70 GHz) and 16 GB of RAM.

The simulations are performed with real road data-based driving scenarios. The acquired data contains the driving information obtained from the bus routes utilized in the public transportation system within Seoul, South Korea. These scenarios capture the real driving environment in Seoul city, considering factors such as traffic conditions and road characteristics.

In the proposed NMPC-based A-ECMS, average travel speed is used to generate reference SOC trajectory, which is utilized when adjusting equivalent factor. The use of the average speed profile to generate the reference SOC trajectory is based on a macroscopic approach, that the driving pattern of target vehicle, FCHEB, adheres to the traffic flow and adopts a pattern similar to the average speed profile. Traffic flow on roads is influenced by various factors such as traffic congestion and driver behavior, leading to changes in traffic characteristics over different time periods. In other words, the NMPC-based A-ECMS is validated against a diverse driving scenarios measured for the target routes at different time periods.

A. DRIVING ROUTE (1): INTRA-CITY BUS

The first driving route used in the simulation is one of the intra-city bus routes in Seoul. These are the mainline buses that operate on major routes connecting main roads

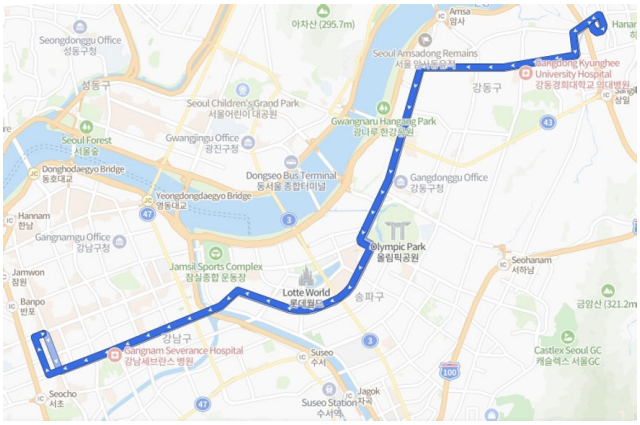

FIGURE 11. The driving route of the intra-city bus applied to the driving scenarios (1-1) and (1-2). This route starts in Gangdong-gu, Seoul and ends in Seocho-gu, Seoul.

and transportation centers. These buses typically cover longer distances and have more bus stops along their routes compared to other bus lines. The target bus in the first scenario covers a total distance of 20.34 km and includes 56 bus stops, as shown in Figure 11. The driving scenarios (1-1) and (1-2) are derived from the data collected during morning and lunch time periods.

1) SCENARIO (1-1): MORNING (LIGHT TRAFFIC)

The first driving scenario for the intra-city bus's route is constructed using the speed profile acquired from 6:30 to 7:53. This scenario (1-1) is measured during the morning time period, covering a total travel time of 5033 s and a distance of 20276.5 m.

The real-driving speed profile and the average travel speed profile for scenario (1-1) are presented in Figure 12. The reference SOC trajectory generated by DP(1), DP(2), and NMPC is shown in Figure 13. The NMPC result does not precisely match with the global optimal solution of DP(1). This is because NMPC relies on an average speed profile and does not have precise knowledge of detailed driving patterns such as stops or accelerations. However, NMPC generates the reference SOC trajectory that takes into account several factors, such as road gradient and traffic flow speed, by considering the driving power profile calculated based on the average travel speed profile. This allows NMPC to exhibit similar trends with that of DP(1).

The results of the DP(1)-based A-ECMS are presented in Figure 14. The results of the DP(2)-based A-ECMS are presented in Figure 15. The results of the NMPC-based A-ECMS are shown in Figure 16. It is evident that all three A-ECMS variants effectively track the reference SOC trajectories computed by DP(1), DP(2) and NMPC. It is important to note that the reference SOC trajectory shown in the simulation results is not based on travel distance, but based on travel time, as indicated in Figure 13.

The fuel cell power utilized during the simulations of Figure 14, Figure 15 and Figure 16 is presented in Figure 17. It demonstrates that both the NMPC-based A-ECMS and

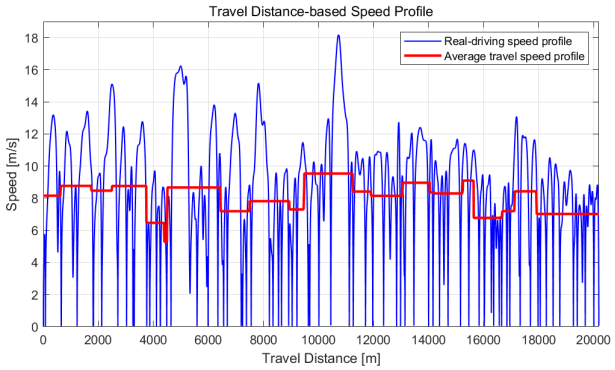

FIGURE 12. Comparison of the travel distance-based speed profile, measured during the morning time period, and the average travel speed profile in driving scenario (1-1). The blue and red lines represent the real driving speed profile and the average travel speed profile.

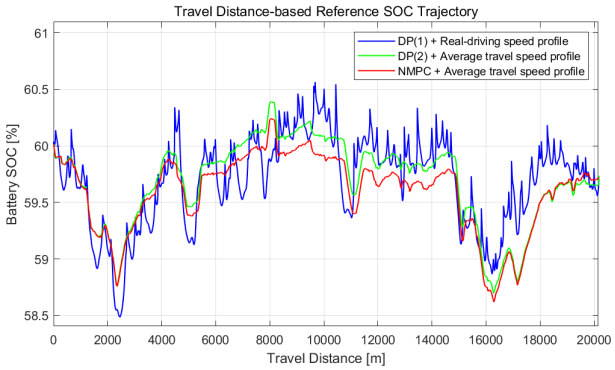

FIGURE 13. Comparison of travel distance-based reference SOC trajectory for driving scenario (1-1). The blue line represents the DP(1) result based on the real driving speed profile. The green and red lines represent the DP(2) result and NMPC result based on the average travel speed profile.

the DP(2)-based A-ECMS utilize excessive fuel cell power compared to the DP(1)-based A-ECMS. This is attributed to the utilization of a reference SOC trajectory that is calculated based on an average speed profile, which is an inaccurate speed profile.

The fuel consumption results and computation time results of DP(1)-based A-ECMS, DP(2)-based A-ECMS, and NMPC-based A-ECMS for scenario (1-1) are presented in Table 3. The rule-based EMS is a controller provided by Autonomie. Even though the rule-based EMS is not a suitable comparison target for the optimal control-based EMS, it is used simply to compare the fuel consumption reduction ratio between DP(1)-based A-ECMS, DP(2)-based A-ECMS, and NMPC-based A-ECMS.

The proposed NMPC-based A-ECMS achieved 0.022 kg higher fuel consumption compared to DP(1). The reason why the fuel consumption of NMPC-based A-ECMS hasn't been minimized as much as the global optimal solution of DP(1) is due to the gap between the average speed profile and the real-driving speed profile.

The proposed NMPC-based A-ECMS resulted in 0.0027 kg higher fuel consumption compared to the results of DP(2), which is generated by considering the same average speed profile and control horizon as NMPC. The reason

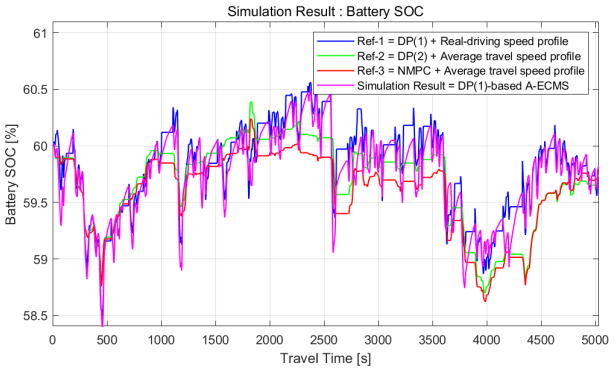

FIGURE 14. Simulation results of battery SOC for DP(1)-based A-ECMS in driving scenario (1-1). The blue, green, and red lines represent travel-time based reference SOC trajectories generated by DP(1), DP(2), and NMPC, respectively. The magenta line represents the simulation results of DP(1)-based A-ECMS, which controls the SOC of the FCHEB to track the reference SOC trajectory generated by DP(1).

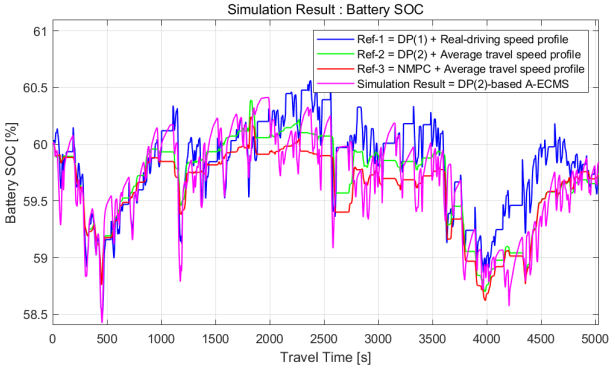

FIGURE 15. Simulation results of battery SOC for DP(2)-based A-ECMS in driving scenario (1-1). The blue, green, and red lines represent travel-time based reference SOC trajectories generated by DP(1), DP(2), and NMPC, respectively. The magenta line represents the simulation results of DP(2)-based A-ECMS, which controls the SOC of the FCHEB to track the reference SOC trajectory generated by DP(2).

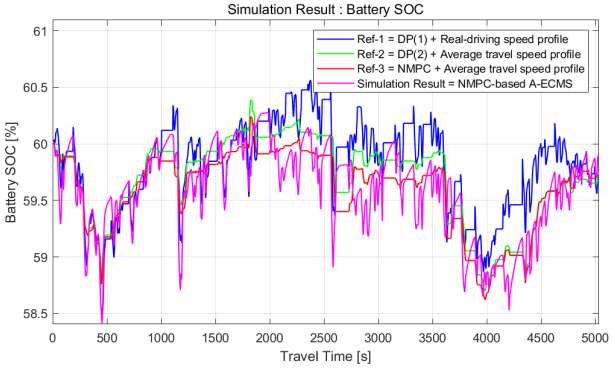

FIGURE 16. Simulation results of battery SOC for NMPC-based A-ECMS in driving scenario (1-1). The blue, green, and red lines represent travel-time based reference SOC trajectories generated by DP(1), DP(2), and NMPC, respectively. The magenta line represents the simulation results of NMPC-based A-ECMS, which controls the SOC of the FCHEB to track the reference SOC trajectory generated by NMPC.

NMPC-based A-ECMS consumed slightly more fuel than the results of DP(2) is due to final SOC was higher at the end of simulation in NMPC-based A-ECMS, amouting to 0.07%.

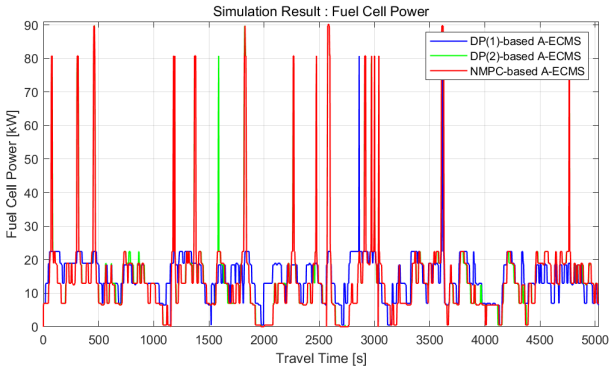

FIGURE 17. Simulation results of fuel cell power for DP(1)-based A-ECMS, DP(2)-based A-ECMS, and NMPC-based A-ECMS in driving scenario (1-1). The blue, green, and red lines represent the simulation results for DP(1)-based A-ECMS, DP(2)-based A-ECMS, and NMPC-based A-ECMS, respectively.

TABLE 3. Comparison of fuel consumption performance in driving scenario (1-1): DP-based A-ECMS and NMPC-based A-ECMS.

Controller	Fuel Consumption / Reduction Rate	Final SOC / Distance	Computation Time
Rule-based EMS	1.0830 kg -	59.82% 20276.5 m	-
DP(1)-based A-ECMS	0.9437 kg 12.858%	59.82% 20276.5 m	15407.76 s
DP(2)-based A-ECMS	0.9630 kg 11.076%	59.84% 20276.5 m	358.84 s
NMPC-based A-ECMS	0.9657 kg 10.831%	59.91% 20276.5 m	0.26 s

Noteworthy result is that the NMPC-based A-ECMS only requires a computation time of 0.26 s, signifying a substantial reduction in computation time compared to that of both DP(1) and DP(2). Through these results, it was validated that the proposed NMPC-based A-ECMS effectively generates the optimal control inputs for the FCHEB within short computation time.

2) SCENARIO (1-2): LUNCH (CONGESTED TRAFFIC)

The second driving scenario for the intra-city bus's route is designed using the speed profile measured during the lunch time period from 13:05 to 14:28. This driving scenario has a total travel time of 5588 s and covers a travel distance of 20320.2 m. Scenario (1-2) involves a travel time that is 600 s longer than scenario (1-1). In other words, scenario (1-2) includes more congested traffic conditions compared to scenario (1-1).

The real-driving speed profile and the average travel speed profile for scenario (1-2) are presented in Figure 18. The reference SOC trajectory generated by DP(1), DP(2), and NMPC is shown in Figure 19. The NMPC results for scenario (1-2) exhibit a similar trend with the global optimal solution of DP(1). However, the deviation between the NMPC and DP(1) results is larger in scenario (1-2) compared to scenario (1-1). This is because traffic congestion is heavier in scenario(1-2) than scenario(1-1).

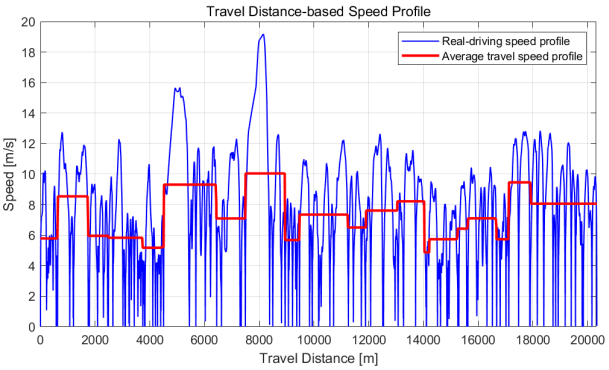

FIGURE 18. Comparison of the travel distance-based speed profile, measured during the lunch time period, and the average travel speed profile in driving scenario (1-2). The blue and red lines represent the real driving speed profile and the average travel speed profile.

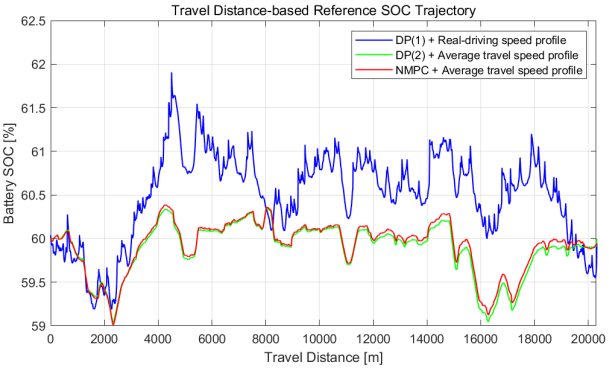

FIGURE 19. Comparison of travel distance-based reference SOC trajectory for driving scenario (1-2). The blue line represents the DP(1) result based on the real driving speed profile. The green and red lines represent the DP(2) result and NMPC result based on the average travel speed profile.

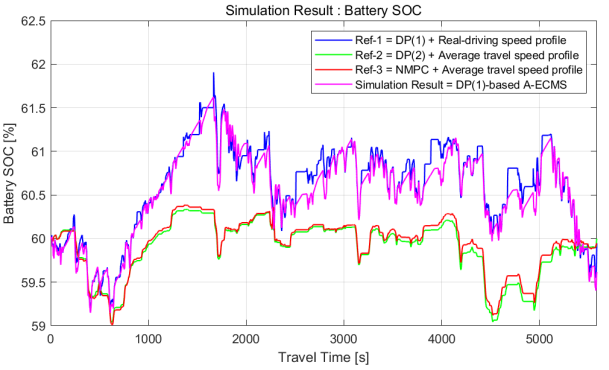

FIGURE 20. Simulation results of battery SOC for DP(1)-based A-ECMS in driving scenario (1-2). The blue, green, and red lines represent travel-time based reference SOC trajectories generated by DP(1), DP(2), and NMPC, respectively. The magenta line represents the simulation results of DP(1)-based A-ECMS, which controls the SOC of the FCHEB to track the reference SOC trajectory generated by DP(1).

The results of the DP(1)-based A-ECMS are presented in Figure 20. The results of the DP(2)-based A-ECMS are presented in Figure 21. The results of the NMPC-based A-ECMS are shown in Figure 22. It is evident that all three A-ECMS variants effectively track the reference SOC

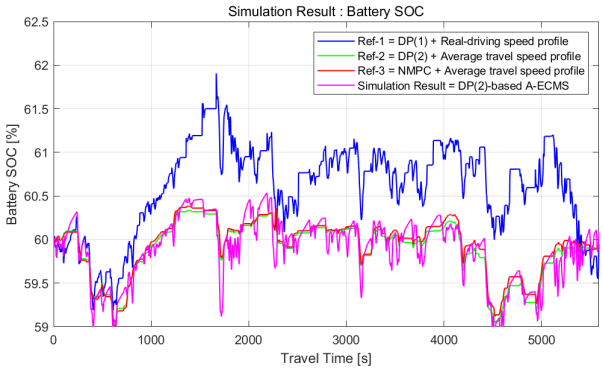

FIGURE 21. Simulation results of battery SOC for DP(2)-based A-ECMS in driving scenario (1-2). The blue, green, and red lines represent travel-time based reference SOC trajectories generated by DP(1), DP(2), and NMPC, respectively. The magenta line represents the simulation results of DP(2)-based A-ECMS, which controls the SOC of the FCHEB to track the reference SOC trajectory generated by DP(2).

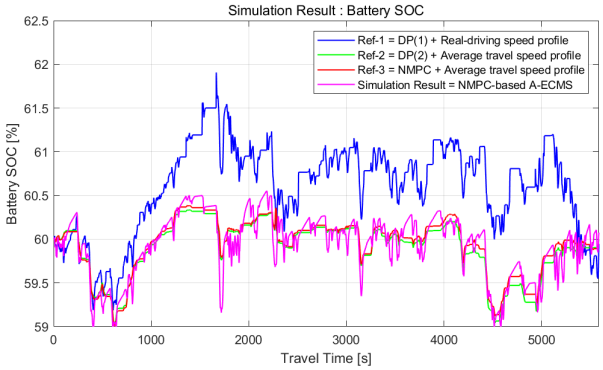

FIGURE 22. Simulation results of battery SOC for NMPC-based A-ECMS in driving scenario (1-2). The blue, green, and red lines represent travel-time based reference SOC trajectories generated by DP(1), DP(2), and NMPC, respectively. The magenta line represents the simulation results of NMPC-based A-ECMS, which controls the SOC of the FCHEB to track the reference SOC trajectory generated by NMPC.

trajectories computed by DP(1), DP(2) and NMPC. It is important to note that the reference SOC trajectory shown in the simulation results is based on travel time, not on the travel distance, as indicated in Figure 19.

The fuel cell power utilized during the simulations of Figure 20, Figure 21 and Figure 22 is presented in Figure 23. It demonstrates that both the NMPC-based A-ECMS and the DP(2)-based A-ECMS utilize excessive fuel cell power compared to the DP(1)-based A-ECMS. This is attributed to the utilization of a reference SOC trajectory that is calculated based on an average speed profile, which is an inaccurate speed profile.

The fuel consumption and computation time used by DP(1)-based A-ECMS, DP(2)-based A-ECMS, and NMPC-based A-ECMS for scenario (1-2) are presented in Table 4. The proposed NMPC-based A-ECMS achieved 0.0267 kg higher fuel consumption compared to DP(1). In other words, there is a slightly larger difference between the results of NMPC-based A-ECMS and the results of DP(1) in scenario (1-2), compared to scenario (1-1). This is because traffic congestion was incorporated in scenario (1-2), leading

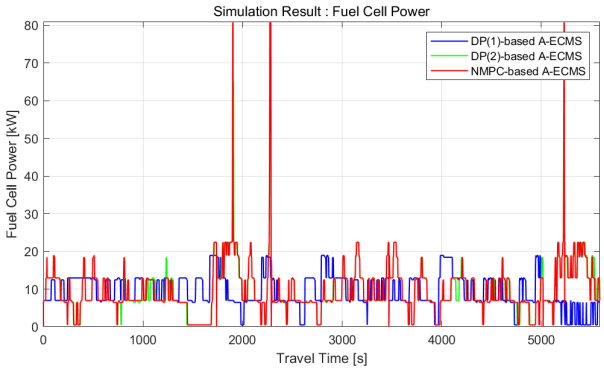

FIGURE 23. Simulation results of fuel cell power for DP(1)-based A-ECMS, DP(2)-based A-ECMS, and NMPC-based A-ECMS in driving scenario (1-2). The blue, green, and red lines represent the simulation results for DP(1)-based A-ECMS, DP(2)-based A-ECMS, and NMPC-based A-ECMS.

TABLE 4. Comparison of fuel consumption performance in driving scenario (1-2): DP(1)-based A-ECMS, DP(2)-based A-ECMS, and NMPC-based A-ECMS.

Controller	Fuel Consumption / Reduction Rate	Final SOC / Distance	Computation Time
Rule-based	0.8106 kg	59.62%	-
EMS	-	20320.2 m	
DP(1)-based	0.6505 kg	59.62%	17098.95 s
A-ECMS	19.746%	20320.2 m	
DP(2)-based	0.6779 kg	60.08%	397.76 s
A-ECMS	16.377%	20320.2 m	
NMPC-based	0.6772 kg	60.07%	0.27 s
A-ECMS	16.461%	20320.2 m	

increase of deviation in the reference SOC trajectory from the global optimal solution.

The proposed NMPC-based A-ECMS resulted in 0.0007 kg less fuel consumption compared to the results of DP(2), which is generated by considering the same average speed profile and control horizon as NMPC. The reason DP(2)-based A-ECMS consumed slightly more fuel than the result of NMPC-based A-ECMS is due to the higher final SOC at the simulation end in DP(2)-based A-ECMS, amounting to 0.01%.

Noteworthy result is that the NMPC-based A-ECMS requires a computation time of 0.28 s, signifying a substantial reduction in computational time compared to both DP(1) and DP(2). Through these results, it was validated that the proposed NMPC-based A-ECMS effectively generates the optimal control inputs for the FCHEB within short computation time.

B. DRIVING ROUTE (1): BRANCH-LINE BUS

The second driving route used in this simulation is one of the branch-line bus routes in Seoul. These buses operate within local routes connecting smaller areas within the city, such as residential neighborhoods. These buses generally travel shorter distances and have fewer bus stops along their routes. The target bus in the second scenario covers a total distance of

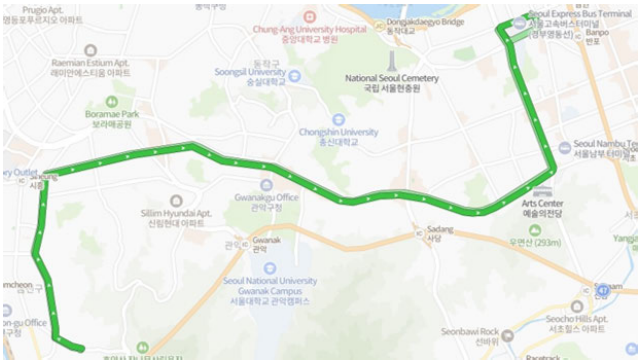

FIGURE 24. The driving route of the branch-line bus applied to the driving scenario (2-1) and (2-2). This route starts in Geumcheon-gu, Seoul and ends at the express bus terminal in Seocho-gu, Seoul.

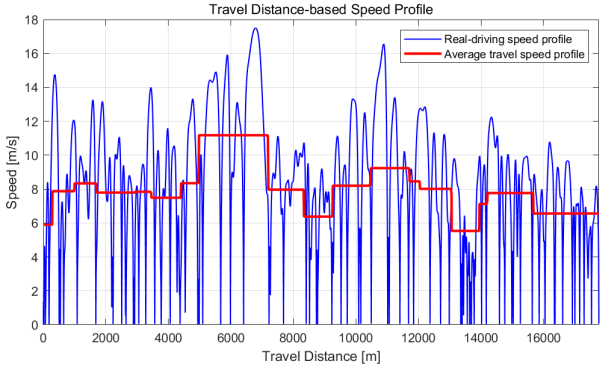

FIGURE 25. Comparison of the travel distance-based speed profile, measured during the morning time period, and the average travel speed profile in driving scenario (2-1). The blue and red lines represent the real driving speed profile and the average travel speed profile.

17.56 km and includes 43 bus stops, as shown in Figure 24. The driving scenarios (2-1) and (2-2) are derived from the data collected during morning and lunch time periods.

1) SCENARIO (2-1): MORNING RUSH HOUR (HEAVY TRAFFIC)

The first driving scenario for the branch-line bus's route is constructed using the speed profile measured during the morning time period from 8:00 to 9:30. This driving scenario has a total travel time of 4884 s and covers a travel distance of 17757.11 m.

The real-driving speed profile and the average travel speed profile for scenario (2-1) are presented in Figure 25. The reference SOC trajectory generated by DP(1), DP(2), and NMPC is shown in Figure 26. The results indicate that NMPC can generate a reference SOC trajectory that exhibits a similar trend with that of DP(1), as demonstrated in driving route (1).

As in driving route (1), the performance of the proposed NMPC-based A-ECMS is validated by comparing it to the DP(1)-based A-ECMS and DP(2)-based A-ECMS. The results of the DP(1)-based A-ECMS are presented in Figure 27. The results of the DP(2)-based A-ECMS are presented in Figure 28. The results of the NMPC-based A-ECMS are shown in Figure 29. It is evident that all three A-ECMS variants effectively track the reference SOC

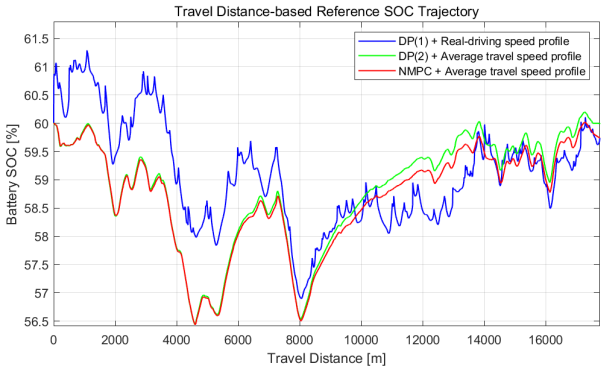

FIGURE 26. Comparison of travel distance-based reference SOC trajectory for driving scenario (2-1). The blue line represents the DP(1) result based on the real driving speed profile. The green and red lines represent the DP(2) result and NMPC result based on the average travel speed profile.

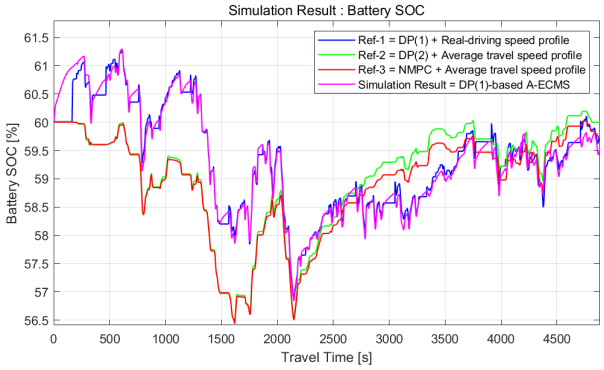

FIGURE 27. Simulation results of battery SOC for DP(1)-based A-ECMS in driving scenario (2-1). The blue, green, and red lines represent travel-time based reference SOC trajectories generated by DP(1), DP(2), and NMPC, respectively. The magenta line represents the simulation results of DP(1)-based A-ECMS, which controls the SOC of the FCHEB to track the reference SOC trajectory generated by DP(1).

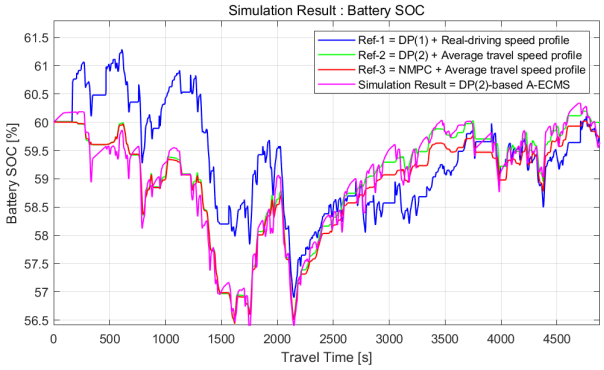

FIGURE 28. Simulation results of battery SOC for DP(2)-based A-ECMS in driving scenario (2-1). The blue, green, and red lines represent travel-time based reference SOC trajectories generated by DP(1), DP(2), and NMPC, respectively. The magenta line represents the simulation results of DP(2)-based A-ECMS, which controls the SOC of the FCHEB to track the reference SOC trajectory generated by DP(2).

trajectories computed by DP(1), DP(2) and NMPC. It is important to note that the reference SOC trajectory shown in the simulation results is based on travel time, not on the travel distance, as indicated in Figure 26.

The fuel cell power utilized during the simulations of Figure 27, Figure 28 and Figure 29 is presented in Figure 30.

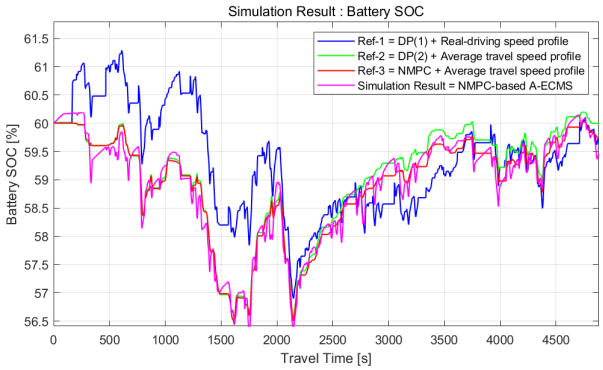

FIGURE 29. Simulation results of battery SOC for NMPC-based A-ECMS in driving scenario (2-1). The blue, green, and red lines represent travel-time based reference SOC trajectories generated by DP(1), DP(2), and NMPC, respectively. The magenta line represents the simulation results of NMPC-based A-ECMS, which controls the SOC of the FCHEB to track the reference SOC trajectory generated by NMPC.

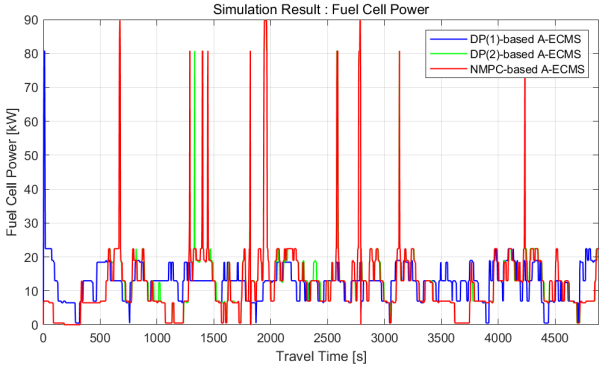

FIGURE 30. Simulation results of fuel cell power for DP(1)-based A-ECMS, DP(2)-based A-ECMS, and NMPC-based A-ECMS in driving scenario (2-1). The blue, green, and red lines represent the simulation results for DP(1)-based A-ECMS, DP(2)-based A-ECMS, and NMPC-based A-ECMS.

It demonstrates that both the NMPC-based A-ECMS and the DP(2)-based A-ECMS utilize excessive fuel cell power compared to the DP(1)-based A-ECMS, as demonstrated in driving scenario (1-1) and (1-2).

The fuel consumption and computation time used by DP(1)-based A-ECMS, DP(2)-based A-ECMS, and NMPC-based A-ECMS for scenario (2-1) are presented in Table 5. The proposed NMPC-based A-ECMS achieved 0.0105 kg higher fuel consumption compared to DP(1). The reason why better performance was shown in scenario (2-1) compared to scenario (1-1) and (1-2) is that it has shorter driving distances and encounters fewer bus stops compared to driving route (1).

The proposed NMPC-based A-ECMS resulted in 0.0081 kg less fuel consumption compared to the results of DP(2), which is generated by considering the same average speed profile and control horizon as NMPC. The reason DP(2)-based A-ECMS consumed slightly more fuel than the result of NMPC-based A-ECMS is due to the higher final SOC at the simulation end in DP(2)-based A-ECMS, amounting to 0.19%.

Noteworthy result is that the NMPC-based A-ECMS requires a computation time of 0.27 s, signifying a substantial reduction in computational time compared to both DP(1) and DP(2). Through these results, it was validated that the proposed NMPC-based A-ECMS effectively generates the optimal control inputs for the FCHEB within short computation time.

TABLE 5. Comparison of fuel consumption performance in driving scenario (2-1): DP-based A-ECMS and NMPC-based A-ECMS.

Controller	Fuel Consumption / Reduction Rate	Final SOC / Distance	Computation Time
Rule-based EMS	0.9380 kg -	59.52% 17757.1 m	-
DP(1)-based A-ECMS	0.7641 kg 18.536%	59.82% 17757.1 m	14215.75 s
DP(2)-based A-ECMS	0.7827 kg 16.560%	59.65% 17757.1 m	331.77 s
NMPC-based A-ECMS	0.7746 kg 17.425%	59.46% 17757.1 m	0.27 s

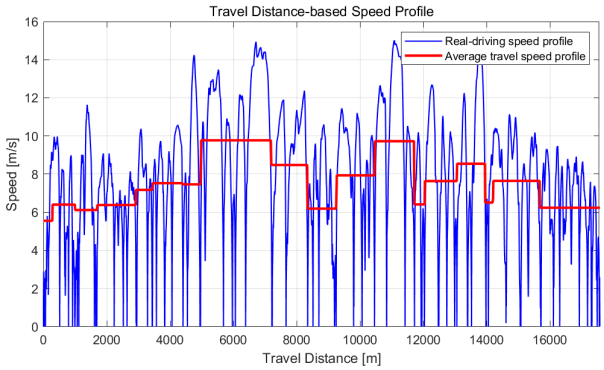

FIGURE 31. Comparison of the travel distance-based speed profile, measured during the lunch time period, and the average travel speed profile in driving scenario (2-2). The blue and red lines represent the real driving speed profile and the average travel speed profile.

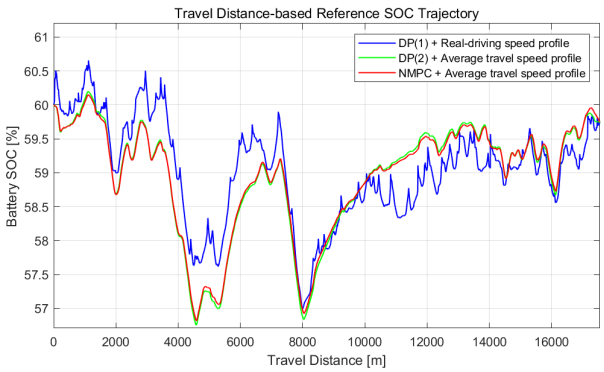

FIGURE 32. Comparison of travel distance-based reference SOC trajectory for driving scenario (2-2). The blue line represents the DP(1) result based on the real driving speed profile. The green and red lines represent the DP(2) result and NMPC result based on the average travel speed profile.

2) SCENARIO (2-2): LUNCH (MEDIUM TRAFFIC)

The second driving scenario for the branch-line bus's route is constructed using the speed profile measured during the lunch time period from 13:30 to 14:43. This driving scenario

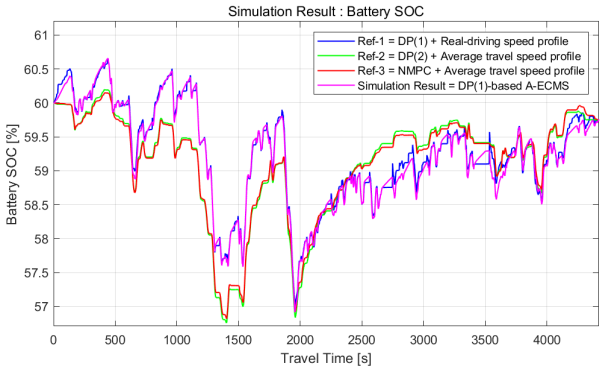

FIGURE 33. Simulation results of battery SOC for DP(1)-based A-ECMS in driving scenario (2-2). The blue, green, and red lines represent travel-time based reference SOC trajectories generated by DP(1), DP(2), and NMPC, respectively. The magenta line represents the simulation results of DP(1)-based A-ECMS, which controls the SOC of the FCHEB to track the reference SOC trajectory generated by DP(1).

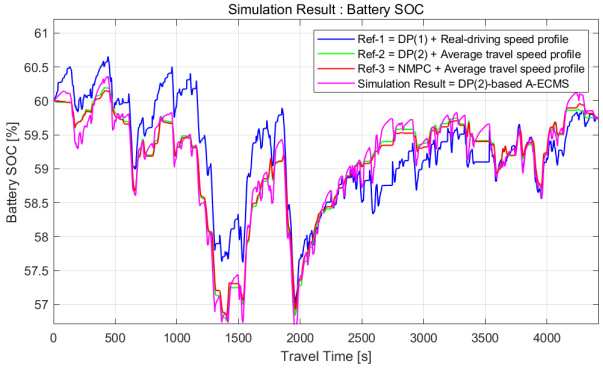

FIGURE 34. Simulation results of battery SOC for DP(2)-based A-ECMS in driving scenario (2-2). The blue, green, and red lines represent travel-time based reference SOC trajectories generated by DP(1), DP(2), and NMPC, respectively. The magenta line represents the simulation results of DP(2)-based A-ECMS, which controls the SOC of the FCHEB to track the reference SOC trajectory generated by DP(2).

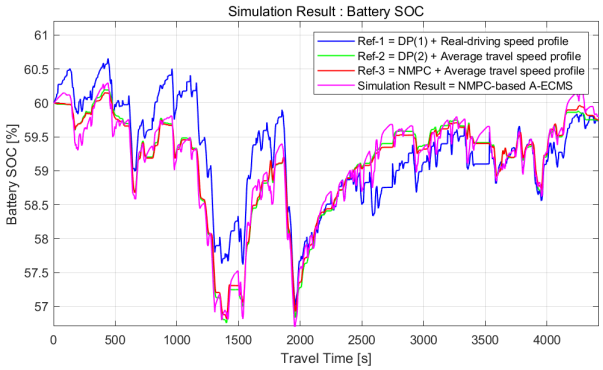

FIGURE 35. Simulation results of battery SOC for NMPC-based A-ECMS in driving scenario (2-2). The blue, green, and red lines represent travel-time based reference SOC trajectories generated by DP(1), DP(2), and NMPC, respectively. The magenta line represents the simulation results of NMPC-based A-ECMS, which controls the SOC of the FCHEB to track the reference SOC trajectory generated by NMPC.

has a total travel time of 4420 s and covers a travel distance of 17555.6 m.

The real-driving speed profile and the average travel speed profile for scenario (2-2) are presented in Figure 31. The reference SOC trajectory generated by DP(1), DP(2), and NMPC is shown in Figure 32. The NMPC results for scenario (2-2) exhibit a similar trend with that of DP(1). Furthermore, the difference between the NMPC and DP(1) results is comparatively smaller for scenario (2-2) than for scenario (2-1). This difference is because traffic congestion is lighter in scenario (2-2) compared to scenario (2-1).

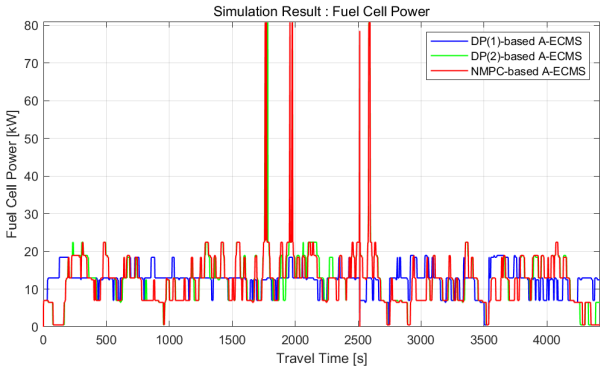

FIGURE 36. Simulation results of fuel cell power for DP(1)-based A-ECMS, DP(2)-based A-ECMS, and NMPC-based A-ECMS in driving scenario (2-2). The blue, green, and red lines represent the simulation results for DP(1)-based A-ECMS, DP(2)-based A-ECMS, and NMPC-based A-ECMS.

As in driving route (1), the performance of the proposed NMPC-based A-ECMS is validated by comparing it to the DP(1)-based A-ECMS and DP(2)-based A-ECMS. The results of the DP(1)-based A-ECMS are presented in Figure 33. The results of the DP(2)-based A-ECMS are presented in Figure 34. The results of the NMPC-based A-ECMS are shown in Figure 35. It is evident that all three A-ECMS variants effectively track the reference SOC trajectories computed by DP(1), DP(2) and NMPC. It is important to note that the reference SOC trajectory shown in the simulation results is based on travel time, not on the travel distance, as indicated in Figure 32.

The fuel cell power utilized during the simulations of Figure 33, Figure 34 and Figure 35 is presented in Figure 36. It demonstrates that both the NMPC-based A-ECMS and the DP(2)-based A-ECMS utilize excessive fuel cell power compared to the DP(1)-based A-ECMS, as demonstrated in driving scenario (1-1), (1-2), and (2-1).

The fuel consumption and computation time used by DP(1)-based A-ECMS, DP(2)-based A-ECMS, and NMPC-based A-ECMS for scenario (2-2) are presented in Table 6. The proposed NMPC-based A-ECMS achieved 0.0099 kg higher fuel consumption compared to DP(1), which generates the global optimal solution by considering the complete driving information in advance.

The proposed NMPC-based A-ECMS resulted in 0.0012 kg higher fuel consumption compared to the results of DP(2), which is generated by considering the same average speed profile and control horizon as NMPC. The reason NMPC-based A-ECMS consumed slightly more fuel than the results of DP(2) is due to the higher final SOC at the

TABLE 6. Comparison of fuel consumption performance in driving scenario (2-2): DP-based A-ECMS and NMPC-based A-ECMS.

Controller	Fuel Consumption / Reduction Rate	Final SOC / Distance	Computation Time
Rule-based	0.8262 kg	59.76%	-
EMS	-	17555.6 m	
DP(1)-based	0.6815 kg	59.76%	12865.05 s
A-ECMS	17.514%	17555.6 m	
DP(2)-based	0.6902 kg	59.77%	334.75 s
A-ECMS	16.469%	17555.6 m	
NMPC-based	0.6914 kg	59.80%	0.25 s
A-ECMS	16.322%	17555.6 m	

simulation end in NMPC-based A-ECMS, amounting to 0.03%.

Noteworthy result is that the NMPC-based A-ECMS requires a computation time of 0.25 s, signifying a substantial reduction in computational time compared to both DP(1) and DP(2). Through these results, it was validated that the proposed NMPC-based A-ECMS effectively generates the optimal control inputs for the FCHEB within short computation time.

V. CONCLUSION AND FUTURE WORK

In this paper, an EMS for the FCHEB that operate as urban public transportation is proposed. The two distinctive features of this EMS are as follows. First, the average speed profiles of road segments included in route of the FCHEB is utilized. Second, the C-rate of battery and the BOP of fuel cell are considered to maintain the durability of the FCHEB. The EMS is based on the NMPC-based A-ECMS, which consists of three main stages: the data pre-processing stage, the NMPC stage, and the A-ECMS stage.

The proposed NMPC-based A-ECMS has been validated in a simulation environment based on four real data-based driving scenarios that incorporate driving speed profiles, average speed profiles, and road gradient profiles obtained from two actual bus routes. And the results of the NMPC-based A-ECMS are compared with those of DP(1) and DP(2). The NMPC-based A-ECMS demonstrated a performance ranging from 95.91% to 98.63% compared to DP(1)'s global optimal solution. Additionally, it achieved equal or superior performance to 99.7% of DP(2)'s optimal solution, which employs the same average driving speed profile and control horizon length used in the NMPC-based A-ECMS. Furthermore, the NMPC-based A-ECMS exhibited a significantly shorter computation time, ranging from 0.25s to 0.27s, in comparison to DP(1) and DP(2). In order words, the proposed NMPC-based A-ECMS effectively generates the optimal control inputs for the FCHEB using the average speed profile within short computation time.

Despite above advantages, the NMPC-based A-ECMS includes one pain points. This issue should be addressed in future work. The issue is use of ideal computational environment. In this paper, The NMPC-based A-ECMS is tested on a computer with abundant computational resources. There is a need for research on how to make NMPC-based A-ECMS work on embedded systems, rather than just in simulation environments. One potential solution could be using AI to learn and operate NMPC-based A-ECMS on these embedded systems.

REFERENCES

[1] A. Chatzipanagi, J. Pavlovic, M. A. Ktistakis, D. Komnos, and G. Fontaras, "Evolution of European light-duty vehicle CO_2 emissions based on recent certification datasets," *Transp. Res. D, Transp. Environ.*, vol. 107, Jun. 2022, Art. no. 103287.

[2] Y. Wang and Z. Huang, "Optimization-based energy management strategy for a 48-V mild parallel hybrid electric power system," *J. Energy Resour. Technol.*, vol. 142, no. 5, May 2020, Art. no. 052002.

[3] M. D. Russo, K. Stutenberg, and C. M. Hall, "Analysis of uncertainty impacts on emissions and fuel economy evaluation for chassis dynamometer testing," *IEEE Trans. Veh. Technol.*, vol. 72, no. 4, pp. 4236–4251, Apr. 2023.

[4] V. Vodovozov, Z. Raud, and E. Petlenkov, "Fuel cell city buses: Grey shadows of green energy," in *Proc. 18th Biennial Baltic Electron. Conf. (BEC)*, Oct. 2022, pp. 1–6.

[5] L. M. Fernandez, P. Garcia, C. A. Garcia, and F. Jurado, "Hybrid electric system based on fuel cell and battery and integrating a single DC/DC converter for a tramway," *Energy Convers. Manage.*, vol. 52, no. 5, pp. 2183–2192, May 2011.

[6] H.-B. Yuan, W.-J. Zou, S. Jung, and Y.-B. Kim, "A real-time rule-based energy management strategy with multi-objective optimization for a fuel cell hybrid electric vehicle," *IEEE Access*, vol. 10, pp. 102618–102628, 2022.

[7] H. Yang, J. Chen, G. Li, and C. Xiao, "Power optimization of hydrogen fuel cell vehicle based on genetic and fuzzy algorithm," in *Proc. 40th Chin. Control Conf. (CCC)*, Jul. 2021, pp. 5853–5856.

[8] Y. Wang, Y. Zhang, C. Zhang, J. Zhou, D. Hu, F. Yi, Z. Fan, and T. Zeng, "Genetic algorithm-based fuzzy optimization of energy management strategy for fuel cell vehicles considering driving cycles recognition," *Energy*, vol. 263, Jan. 2023, Art. no. 126112.

[9] D. Fares, R. Chedid, F. Panik, S. Karaki, and R. Jabr, "Dynamic programming technique for optimizing fuel cell hybrid vehicles," *Int. J. Hydrogen Energy*, vol. 40, no. 24, pp. 7777–7790, Jun. 2015.

[10] S. Tao, W. Chen, R. Gan, L. Li, G. Zhang, Y. Han, and Q. Li, "Energy management strategy based on dynamic programming with durability extension for fuel cell hybrid tramway," *Railway Eng. Sci.*, vol. 29, no. 3, pp. 299–313, Sep. 2021.

[11] L. Xu, M. Ouyang, J. Li, and F. Yang, "Dynamic programming algorithm for minimizing operating cost of a PEM fuel cell vehicle," in *Proc. IEEE Int. Symp. Ind. Electron.*, May 2012, pp. 1490–1495.

[12] C. Liu and L. Liu, "Optimal power source sizing of fuel cell hybrid vehicles based on Pontryagin's minimum principle," *Int. J. Hydrogen Energy*, vol. 40, no. 26, pp. 8454–8464, Jul. 2015.

[13] P. Li, Y. Huangfu, C. Tian, S. Quan, Y. Zhang, and J. Wei, "An improved energy management strategy for fuel cell hybrid vehicles based on the Pontryagin's minimum principle," in *Proc. IEEE Ind. Appl. Soc. Annu. Meeting (IAS)*, Oct. 2021, pp. 1–6.

[14] X. Sun, Y. Zhou, L. Huang, and J. Lian, "A real-time PMP energy management strategy for fuel cell hybrid buses based on driving segment feature recognition," *Int. J. Hydrogen Energy*, vol. 46, no. 80, pp. 39983–40000, Nov. 2021.

[15] C. Zheng, S. W. Cha, Y.-I. Park, W. S. Lim, and G. Xu, "PMP-based power management strategy of fuel cell hybrid vehicles considering multi-objective optimization," *Int. J. Precis. Eng. Manuf.*, vol. 14, no. 5, pp. 845–853, May 2013.

[16] Y. Zhang, M. Chen, S. Cai, S. Hou, H. Yin, and J. Gao, "An online energy management strategy for fuel cell hybrid vehicles," in *Proc. 40th Chin. Control Conf. (CCC)*, Jul. 2021, pp. 6034–6039.

[17] H. Hemi, J. Ghouili, and A. Cheriti, "A real time energy management for electrical vehicle using combination of rule-based and ECMS," in *Proc. IEEE Electr. Power Energy Conf.*, Aug. 2013, pp. 1–6.

[18] H. Li, A. Ravey, A. N'Diaye, and A. Djerdir, "Online adaptive equivalent consumption minimization strategy for fuel cell hybrid electric vehicle considering power sources degradation," *Energy Convers. Manage.*, vol. 192, pp. 133–149, Jul. 2019.
[19] Q. Jiang, O. Bethoux, F. Ossart, E. Berthelot, and C. Marchand, "A-ECMS and SDP energy management algorithms applied to a fuel cell electric scooter," in *Proc. IEEE Vehicle Power Propuls. Conf. (VPPC)*, Dec. 2017, pp. 1–5.
[20] X. Lin, X. Xu, and H. Lin, "Predictive-ECMS based degradation protective control strategy for a fuel cell hybrid electric vehicle considering uphill condition," *eTransportation*, vol. 12, May 2022, Art. no. 100168.
[21] B. Geng, J. K. Mills, and D. Sun, "Two-stage energy management control of fuel cell plug-in hybrid electric vehicles considering fuel cell longevity," *IEEE Trans. Veh. Technol.*, vol. 61, no. 2, pp. 498–508, Feb. 2012.
[22] X. Li, Y. Wang, D. Yang, and Z. Chen, "Adaptive energy management strategy for fuel cell/battery hybrid vehicles using Pontryagin's minimal principle," *J. Power Sources*, vol. 440, Nov. 2019, Art. no. 227105.
[23] J. Guo, H. He, Z. Wei, and J. Li, "An economic driving energy management strategy for the fuel cell bus," *IEEE Trans. Transport. Electrific.*, early access, Jun. 22, 2022, doi: 10.1109/TTE.2022.3185215.
[24] D. F. Pereira, F. D. C. Lopes, and E. H. Watanabe, "Nonlinear model predictive control for the energy management of fuel cell hybrid electric vehicles in real time," *IEEE Trans. Ind. Electron.*, vol. 68, no. 4, pp. 3213–3223, Apr. 2021.
[25] H. Chen, J. Chen, H. Lu, C. Yan, and Z. Liu, "A modified MPC-based optimal strategy of power management for fuel cell hybrid vehicles," *IEEE/ASME Trans. Mechatronics*, vol. 25, no. 4, pp. 2009–2018, Aug. 2020.
[26] H. He, S. Quan, F. Sun, and Y.-X. Wang, "Model predictive control with lifetime constraints based energy management strategy for proton exchange membrane fuel cell hybrid power systems," *IEEE Trans. Ind. Electron.*, vol. 67, no. 10, pp. 9012–9023, Oct. 2020.
[27] C. Ziogou, S. Voutetakis, M. C. Georgiadis, and S. Papadopoulou, "Model predictive control (MPC) strategies for PEM fuel cell systems—A comparative experimental demonstration," *Chem. Eng. Res. Des.*, vol. 131, pp. 656–670, Mar. 2018.
[28] T. Li, H. Liu, H. Wang, and Y. Yao, "Multiobjective optimal predictive energy management for fuel cell/battery hybrid construction vehicles," *IEEE Access*, vol. 8, pp. 25927–25937, 2020.
[29] X. Lin, Z. Wang, S. Zeng, W. Huang, and X. Li, "Real-time optimization strategy by using sequence quadratic programming with multivariate nonlinear regression for a fuel cell electric vehicle," *Int. J. Hydrogen Energy*, vol. 46, no. 24, pp. 13240–13251, Apr. 2021.
[30] M. Yan, G. Li, M. Li, H. He, H. Xu, and H. Liu, "Hierarchical predictive energy management of fuel cell buses with launch control integrating traffic information," *Energy Convers. Manage.*, vol. 256, Mar. 2022, Art. no. 115397.
[31] M. Salem, M. Elnaggar, M. S. Saad, and H. A. A. Fattah, "Energy management system for fuel cell-battery vehicles using multi objective online optimization," *IEEE Access*, vol. 10, pp. 40629–40641, 2022.
[32] J. Díaz-Ramirez, N. Giraldo-Peralta, D. Flórez-Ceron, V. Rangel, C. Mejía-Argueta, J. I. Huertas, and M. Bernal, "Eco-driving key factors that influence fuel consumption in heavy-truck fleets: A Colombian case," *Transp. Res. D, Transp. Environ.*, vol. 56, pp. 258–270, Oct. 2017.
[33] J. Gao, H. Chen, Y. Li, J. Chen, Y. Zhang, K. Dave, and Y. Huang, "Fuel consumption and exhaust emissions of diesel vehicles in worldwide harmonized light vehicles test cycles and their sensitivities to eco-driving factors," *Energy Convers. Manage.*, vol. 196, pp. 605–613, Sep. 2019.
[34] C. Flores, P. Merdrignac, R. de Charette, F. Navas, V. Milanés, and F. Nashashibi, "A cooperative car-Following/Emergency braking system with prediction-based pedestrian avoidance capabilities," *IEEE Trans. Intell. Transp. Syst.*, vol. 20, no. 5, pp. 1837–1846, May 2019.
[35] H. S. Bae and J. C. Gerdes, "Command modification using input shaping for automated highway systems with heavy trucks," in *Proc. Amer. Control Conf.*, vol. 1, 2003, pp. 54–59.
[36] L. T. Biegler and V. M. Zavala, "Large-scale nonlinear programming using IPOPT: An integrating framework for enterprise-wide dynamic optimization," *Comput. Chem. Eng.*, vol. 33, no. 3, pp. 575–582, Mar. 2009.
[37] J. A. E. Andersson, J. Gillis, G. Horn, J. B. Rawlings, and M. Diehl, "CasADi: A software framework for nonlinear optimization and optimal control," *Math. Program. Comput.*, vol. 11, no. 1, pp. 1–36, Mar. 2019.
[38] H. Liu, R. Liu, R. Xu, L. Han, and S. Ruan, "Hierarchical energy management strategy considering switching schedule for a dual-mode hybrid electric vehicle," *Proc. Inst. Mech. Eng. D, J. Automobile Eng.*, vol. 236, no. 5, pp. 938–949, Apr. 2022.
[39] J. T. B. A. Kessels, M. W. T. Koot, P. P. J. van den Bosch, and D. B. Kok, "Online energy management for hybrid electric vehicles," *IEEE Trans. Veh. Technol.*, vol. 57, no. 6, pp. 3428–3440, Nov. 2008.
[40] T. Ghandriz, B. Jacobson, N. Murgovski, P. Nilsson, and L. Laine, "Real-time predictive energy management of hybrid electric heavy vehicles by sequential programming," *IEEE Trans. Veh. Technol.*, vol. 70, no. 5, pp. 4113–4128, May 2021.
[41] Argonne National Laboratory. (2018). *Autonomie*. Accessed: Jul. 20, 2023. [Online]. Available: https://www.anl.gov/

JOOIN LEE received the B.S. degree in mechanical engineering from Soongsil University, Seoul, South Korea, in 2015. He is currently pursuing the Ph.D. degree in electrical engineering with Hanyang University, Seoul. His current research interests include model predictive control, optimal hybrid powertrain control, fault-tolerant control, and applications to vehicle control.

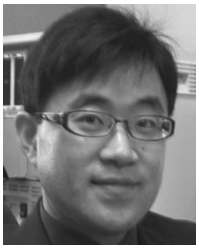

HYEONGCHEOL LEE (Member, IEEE) received the B.S. and M.S. degrees from Seoul National University, Seoul, South Korea, in 1988 and 1990, respectively, and the Ph.D. degree from the University of California at Berkeley, Berkeley, CA, USA, in 1997. He is currently a Professor with the Department of Electrical and Biomedical Engineering, Hanyang University, Seoul. His research interests include adaptive and nonlinear control, embedded systems, applications to vehicle control, and vehicle dynamics.